UNIVERSIDADE DA BEIRA INTERIOR
Engenharia

Design of a Monosized Droplet Generator
Versão final após defesa

Cátia Isabel Neves Moura

Dissertação para obtenção do Grau de Mestre em
Engenharia Aeronáutica
(Ciclo de estudos integrado)

Orientador: Prof. Doutor André Resende Rodrigues da Silva

Covilhã, julho de 2020

Acknowledgements

First of all, I would like to thank my parents for never giving up on me besides all adversity. Without them, none of my accomplishments would be a reality.

Secondly, I would like to show my sincere gratitude to my supervisor, André Silva, for allowing me to be a part of his team, for allowing me to develop my capabilities as a researcher and for boosting me to grow as a human being.

I also like to thank and acknowledge AEROG - Aeronautics and Astronautics Research Center, as well as all my colleges that made this whole process easier, especially Emanuel Camacho for all the support and friendship.

I would also like to gratify the lab technician Mr. Rui Manuel Tomé Paulo who was a resourceful help throughout the development of this work.

Resumo

Esta dissertação foca-se no desenvolvimento e validação de um instrumento que permite a formação de gotas. Este documento começa por mostrar o design desenvolvido para este propósito. Após o desenvolvimento do design, as peças foram construídas recorrendo à impressão 3D. Após a impressão das peças, procedeu-se à montagem e validação do dispositivo. Para a validação deste instrumento, foi necessário criar uma estação de testes que é mostrada no capítulo 3. Após todo o processo de montagem, realizaram-se os testes de validação.

Na fase de validação, usou-se água para a validação do aparelho. Seis caudais diferentes foram implementados, de forma a determinar o efeito do caudal na formação e comportamento das gotas. Os resultados destes testes foram obtidos através de métodos de visualização. Após todas as imagens serem recolhidas na fase de testes, estas foram analisadas para a extracção de diâmetros. Depois deste processo ter sido concluido, procedeu-se a testar a geração de gotas perturbada. Nesta fase de testes, três caudais foram escolhidos de entre os im,postos na primeira fase de validação e impostos. Os caudais escolhidos para a fase perturbada da geração de gotas foram: 2.5, 4 e 5 ml/min. O procedimento para estes testes foi a implementação do caudal e do sinal. Após a implementação do caudal, a onda electromagnética foi construída para implementar na célula piezoeléctrica. O sinal electromagnético consiste numa onda quadrada de amplitude constante (20 Vpp), onde a frequência é periodicamente aumentada.

O estudo com várias frequências visa a investigação da influência da frequência na formação de gotas para o caso deste instrumento. Este estudo permite testar se o aparato é capaz de criar gotas consecutivas com alta repetibilidade no que toca a diâmetros e espaçamento entre gotas. À semelhança dos casos não perturbados, a formação perturbada de gotas também foi testada através de visualização e análise de imagem.

Palavras-chave

Piezoelectricidade; Produção consecutica de gotas; Monodispersão.

Abstract

This dissertation focuses on the development and validation of an instrument that allows the formation of drops. This document starts by showing the design developed for this purpose. After the development of the design, the pieces were built using 3D printing. When the process was complete, the device was assembled and validated. For the validation of this instrument, it was necessary to create a test station which is shown in chapter 3. After the entire assembly process, the validation tests were carried out.

In the validation phase, water was applied to be ejected by the apparatus. Six different flow rates were implemented in order to determine the effect of the flow rate on the formation and behavior of the drops. The results of these tests were obtained through visualization methods. After all the images were collected in the testing phase, they were analyzed for the extraction of diameters. After the tests of undisturbed droplet formation were completed, the disturbed generation of droplets was proceeded to test. In this testing phase, three flows were chosen from the previous phase and imposed. The flow rates chosen for the disturbed phase of the generation of droplets were: 2.5, 4 and 5 ml/min. The proceedings for these tests was the flow and signal implementation. After the flow was implemented, the electromagnetic wave was built to be implemented in the piezoelectric cell. The electromagnetic signal consists of a square wave of constant amplitude (20 Vpp), where the frequency is periodically increased.

The study with several frequencies aims to investigate the influence of frequency on the formation of drops for the case of this instrument. This study allows testing whether the apparatus is capable of creating consecutive drops with high repeatability in terms of diameter and spacing between drops. Like the undisturbed cases, the disturbed droplet formation was also tested through visualization and image analysis.

Keywords

Piezoelectricity; Stream droplet breakup; Monodispersity.

Contents

List of Figures

List of Tables

Acronym List

Nomenclature

A	Area of the nozzle
Bo	Bond number
Ca	Capillary number
D1	Diameter of the copper plate
D2	Diameter of the piezoelectric ceramic
$\mathrm{D_d}$	Diameter of the droplet
$\mathrm{D_n}$	Diameter of the nozzle
g	Gravitational acceleration
PHB	Pinhole Holder Base
PHL	Pinhole Holder Lid
Q	Applied flow rate
Re	Reynolds number
t	Thickness of the piezoelectric diaphragm
U	Fluid velocity at the nozzle
We	Weber number
$\mathrm{We_{cr}}$	Critical Weber number
F_E	Electrical Force
q	Charge of the Particle
E	Magnitude of the Electric Field

Greek Symbols

μ	Dynamic viscosity
ρ	Density
σ	Surface tension

Subscripts

n	Related to nozzle
cr	Related to We - critical
d_x	Related to drop

Acronyms

CAD	Computer Aided Design
DC	Direct Current
DOD	Drop on Demand
EHDA	Electro-Hydrodynamic Atomization
fps	Frames per second
LED	Light Emitting Diode
MDG	Micro Drop Generators
MEMS	Micro-Electromechanical Systems
NEMS	Nano-Electromechanical Systems

Chapter 1

Introduction

This chapter presents a glimpse of the motivations and objectives for the realization of this work. Also present in this chapter, a review of the related concepts is provided. Initially, the different devices of spray generation and respective details are shown. Later on, a brief literature review is presented, where the droplet generation concepts used in previously developed investigations, as well as the corresponding results and conclusions, are provided.

1.1 Outline

This document starts by listing the motivation and objectives of the present work. These topics are detailed throughout the first chapter. Later on, still in the first chapter, a brief explanation of droplet generation concepts is provided. This section regards both the dimensionless numbers that characterize droplet generation and the droplet generation mechanisms. Later, on the following section, an overview of the different pre-existent droplet generators is shown, where different artificially assisted droplet generators are explained. Furthermore, in the last section of the present chapter, a literature review on piezoelectric droplet generators is provided, where past works on the matter are analysed.

Advancing to chapter 2, the proposed device and validation facilities are shown. In this chapter, the designed parts and acquired components of the proposed device are shown. Also in this chapter, the experimental facilities are shown and the characteristics of every component are found. Furthermore, in the final part of chapter 2, the steps of the testing and data extraction processes are meticulously traced.

Chapter 3 presents the results of the device testing and a small characterization of the device for the applied conditions. In this chapter, the different phenomena found throughout this investigation are shown and explained. Further on the chapter, the analysis of the extracted data is presented by crossing the visualization information with graphical representations.

Finally, the conclusions and future work are shown (chapter 4).

1.2 Motivation

This dissertation reports the development and validation of a micro-droplet spray generator. For this objective, this document proposes a new configuration for creating micro-droplets, in a controlled manner. The device recurs to the use of materials with piezoelectric characteristics. In this work, validation and characterization of the device are provided, further-after.

The interest in studying droplet behaviour has been increasing over the last decades. On the dispensing industry, a major problem was and still is, to this day, aiming to minimize droplet diameter and to eject droplets in a controlled manner. Micro-dispensing has gained its popularity for its multiple applications, such as biotechnology and manufacturing engineering. Fuel

dispensing in auto and aero-engine technology is no different from these last enunciated applications. The atomization of fuels is a way to optimize combustion. Optimization of the combustion process means that the gas emission decreases.

For this motive, it is important to study the behaviour of atomized fluids. This dissertation presents a new design and configuration to a fluid micro-dispenser. After development, this device should be able to create micro-sized droplets of various fluids. The capability to create micro-droplets allows the study of the behaviour of fluids on a micro-scale. This device is created to improve knowledge about the behaviour of the fluids in several conditions. This allows the usage of this kind of devices in several applications.

1.3 Objectives

Throughout the years, micro-dispensing has aroused some attention due to its potential in several areas. In this case, the main objective of this dissertation is to create a new design of a droplet generator to create streams of droplets with well-defined diameters. After the design is complete, the device must be built and validated. During the validation, several objectives arise. The main objective is to find out if the proposed design allows the user to control the droplet diameter. From there, another objective arises: verify if the device can generate sequences of monosized droplets in a controlled manner. Another objective is the characterization of the device in different regimens and to define the ranges of monodispersity.

1.4 Overview

The study of droplet formation dates back over a century, as well as its multiple utilities for engineering and investigation purposes. Currently, the main studies in the droplet generation field are focused on micro-monodisperse dispensing [1]. When talking about droplet dispensing systems, a group of variables needs to be taken into account, such as fluid properties and environmental conditions. Throughout the development of the dispensing industry, many dispenser configurations were created. These dispensers recurred to different mechanisms to reach droplet formation. the droplet generation devices can be classified according to their ejecting mechanisms, configurations and the applied disturbance source.

Two of the most recognized droplet formation mechanisms are the dripping and continuous jet breakup. These two methods are achieved naturally but the interest to obtain uniform droplets increased, and with that, some new mechanisms emerged: Drop-on-demand (DOD) and Stream droplet formation. These last processes are usually achieved recurring to assisted droplet breakup. In DOD mode, the meniscus needs to be stable at the nozzle plan when the pressure pulse is applied. The pendant droplet, generated outwards of the nozzle, is released from the nozzle when the membrane is no longer under the effect of the applied signal, causing the fluid at the nozzle to withdraw towards the interior of the fluid container. Gradually increasing the liquid flow, the ejection regime changes with the increase of the Webber number, creating a laminar jet (Fig. 1.3b). By action of the signal, generated by the sound source, the jet suffers an additional mechanical disturbance that propagates exponentially over the jet. When the effect of the actuating disturbances is so big that the gravitational forces overcome the surface tension forces pinch-off occurs. On pinch-off point a droplet with the same volume

of the portion of the jet corresponding to the wavelength of the sound signal. In this generation mode, at optimal disturbance conditions, a stream of uniform-sized droplets should be observed. When working at a non-optimal signal, one can observe the formation of satellite droplets and/or coalescence of droplets.

Depending on the applied disturbance source, the devices can be labelled as thermoelectric, acoustic, pneumatic, microfluidic, electro-hydrodynamic or piezoelectric droplet generators. The following subsections provide insight into different types of devices concerning the disturbance type labelling.

1.4.1 Droplet Generation

In this section, the fundamentals of droplet generation are addressed. This section starts by listing the dimensionless numbers that characterize the generation of droplets. Moving forward, an explanation of the different droplet formation phenomena is provided.

1.4.1.1 Governing Parameters

Several studies were performed prior to this experiment. Those studies aim to investigate droplet generation under different circumstances. In order to find the experiment conditions, some dimensionless numbers were developed that characterize droplet formation. Usually, droplet formation is characterized by the Bond (Bo), Capillary (Ca) and Reynolds (Re) number.

Equation 1.1 shows the Bond number that represents a ration between the forces suffered by the droplet and the forces resulting from the surface tension. Then the Capillary is shown, in equation 1.2, is the relation between the forces of viscosity and surface tension. The Reynolds number also presents an important role in the characterization of droplet formation and is shown in equation 1.3. This last number represents the ratio between the inertial and viscous forces.

$$Bo = \frac{\rho g D_d^2}{\sigma} \quad (1.1)$$

$$Ca = \frac{\mu}{\sigma} U \quad (1.2)$$

$$Re = \frac{\rho U D_d}{\mu} \quad (1.3)$$

The droplet generation characterization parameters are shown in the equations above. For these values, ρ represents the density of the ejected fluid, g stands for the gravitational acceleration, D_d is the diameter of the droplet, σ is the surface tension and μ is the dynamic viscosity of the fluid. U stands for the velocity of the fluid that is given by $U = Q/A$, where Q is the flow rate and A correspond to the area of the nozzle which, in this case, is given by $A = \pi D_n^2$, with D_n being the diameter of the nozzle. When talking about jets, another dimensionless number pops up that is used to characterize the jetting mode, the Weber number. The Weber number

is characterized by the ratio between the kinetic energy and the surface energy and is shown in equation 1.4.

$$We = \frac{\rho U^2 D_d}{\sigma} = CaRe \quad (1.4)$$

1.4.1.2 Droplet Generation Mechanisms

As mentioned before in this document, there are multiple droplet generation mechanisms: Dripping, continuous jetting, DOD and controlled stream jet-breakup. The first two are the ones we encounter naturally. They are defined according to the droplet generation rate and are highly dependant on the applied flow rate [2]. As the years go by, the dispensing industry became focused on minimizing the droplet diameters and controlling the droplet generation rate. Due to this interest, new mechanisms were developed to solve this problem. It is then that DOD and controlled stream jet-breakup arise.

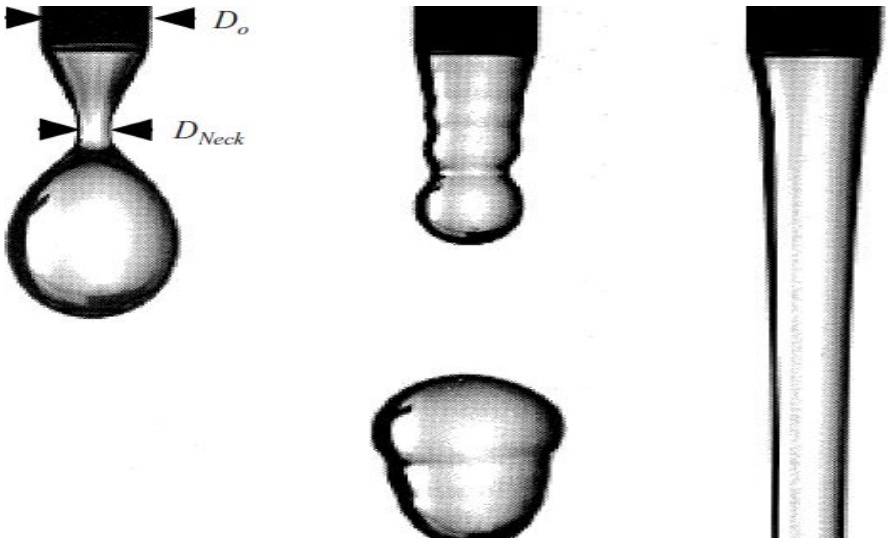

Figure 1.1: Droplet generation mechanisms [3].

The simplest way to create single droplets is by dripping mode. This process consists of slow ejection of fluid through the nozzle (e.g., needle), which causes fluid deposition on the outside of the nozzle. Due to the deposition, a slow-growing pending mass of fluid is generated. This growth happens due to the surface tension forces of the fluid. During the growth of the pendant droplets, the accumulation of fluid is characterized by the equilibrium between inertial and surface tension forces [4]. After some time, the droplet achieves a critical size and is released. This occurs because the surface tension and inertial forces no longer overcome the gravitational force [2, 3, 5]. This droplet generation mechanism implies low production rates and larger droplet diameters which are mainly influenced by the shape and size of the nozzle orifice [2, 3, 5–10].

In 1985, a new droplet generations mechanism was defined inside the dripping mode [11]. This meant that the dripping mode was divided into two differently defined states: periodic dripping and dripping faucet. The periodic dripping was defined as periodically producing droplets of roughly the same characteristics (Fig. 1.1a). This way of droplet generation was defined by

Weber numbers much smaller than one [12, 13]. Still inside the dripping mode, but characterized by bigger Weber numbers, the dripping faucet was defined, around 1985, as chaos dripping state. This definition was applied because the almost spherical form no longer was applied to the pending droplet and the generated droplets had distinct releasing times and sizes. This droplet generation mechanism is shown in figure 1.1b.

When the flow rate is gradually increased to a point where the fluid velocity U, is such that the kinetic energy overcomes the surface energy, a continuous jet is created (Fig. 1.1c). This new state is called jetting. For the jetting mechanism to take place, the breakup of droplets moves away from the droplets to take place downstream [3, 14]. In this state, a column of fluid forms to later pinch of into droplets by the effect of capillary instabilities [15]. These instabilities are commonly referred to as Rayleigh instabilities [3]. The most common definitions for this dispensing mechanism are the high applied flow rates and droplet generation rates, but the parameter that can numerically define it is the Weber number. Some authors defined the critical point of Weber number, for which the droplet generation transitions from dripping mode to jetting, as:

$$We_{cr} = \frac{\rho U^2 D}{\sigma} \approx 0.8 \quad (1.5)$$

In order to solve size and generation rate associated troubles of single droplet formation, a well-defined disturbance needs to be applied in the fluid chamber or on the fluid to anticipate the droplet formation, enhancing the generation rate and diameter. To this day several disturbances have been reported as droplet generator actuators such as thermoelectric, piezoelectric, acoustic, pneumatic, microfluidic, electro-hydrodynamic and aerodynamic [16]. In all the types of generators mentioned above, the generation rate is dependent on the disturbance descendant from the signal applied. This dependence enables the device to work with slightly higher droplet generation rates when compared to undisturbed generators. The different types of disturbance are clearly explained in section 1.4. This droplet generation method is common in nature and human beings have been using it since the early days without even noticing it. Showerheads, leaking taps and some gardening tools are some examples of day to day uses of stream droplet generation.

Drop-on-demand generators consist of dispensing single droplets in a controlled manner. The concept between DOD generators is to apply a specific punctual disturbance at a low flow rate. The concept is close to dripping mode. The application of a disturbance allows the operator to control the size and time of the droplet generation [17]. Usually, in this kind of droplet generation, the disturbance implies pressure fluctuations on the fluid container. The pressure on the fluid chamber increases and a small portion of the fluid is pushed through the nozzle. Then, the pressure on the chamber returns to its initial value, creating a negative pressure difference. The pressure differential on the fluid chamber results in the withdrawing of the fluid back into the fluid chamber, causing the pendant portion of the fluid to break into a droplet. By applying a disturbance, the diameter and time of production of the droplet decrease. This way, relating to the natural dripping, the droplet size is roughly controllable, since the pendant droplet does not have the time to form into a bigger droplet. The effects of the disturbance, in this case, come to assist the effects of the gravitational force [16]. Inertial disturbances are also applied to this type of droplet generator.

Another way to create droplets is through a controlled jet breakup. Several studies have been performed during the past century on droplet formation from jet breakups such as Rayleigh and Millikan. However, in high accuracy requirement applications and higher generation rate, well-defined trajectories and size repeatability are more desirable when compared to random aerosol generation. To accomplish micro-droplets in a monodisperse generation, one must be able to create high-speed jets with a diameter of the same order of magnitude of the desired droplet diameter. For this kind of droplet generating it is necessary to accurately control the behaviour of the jet, regarding the breakup, to reach uniform-sized droplets [17]. The main principle behind this method of droplet generation is to implement an intermittent disturbance to a fluid being ejected under jet form [13]. The application of the disturbance causes the necks of the jet to decrease the diameter. This way, the jet breaks into droplets sooner. For this reason, the length of the jet is smaller [18].

1.4.2 Disturbance Assisted Droplet Generators

This section provides a detailed explanation of the different types of droplet generators that recur to artificial disturbance. For this purpose Thermoelectric, Acoustic, Microfluidic, Electro-Hydrodynamic and Piezoelectric droplet generators are detailed.

1.4.2.1 Thermoelectric Droplet Generators

Thermoelectric droplet generators, also known as bubble jet droplet generators, employ thermoelectric technology in droplet generation and are commonly used in ink-jet printing technology. In this DOD technology, droplet formation is achievable by applying a short duration electric pulse to a resistive component, in contact with the fluid. The resistor is usually placed near the ejection aperture or in the wall of the fluid chamber. Its resistive properties cause the component to heat, increasing the fluid temperature to a metastable point [19] where gas bubble nucleation is presented as shown in figure 1.2. The coalescence of nucleated bubbles create a growing gaseous sheet (Fig. 1.2c) and, by consequence of increased pressure in the chamber, a pendant of fluid is created in the nozzle due to a pressure pulse. The pending fluid is released when the bubble sheet reaches its maximal dimensions (Fig. 1.2d) and collapses (Fig. 1.2e). Due to the actuating capillary forces, after the bubble collapse occurs a refilling of the nozzle as can be seen in figure 1.2f.

Nucleation is the phase of the thermal droplet dispensing cycle where the gas bubble nuclei are formed, the gaseous sheet grows and small pressure fluctuations are noticeable on the fluid chamber. This process is visible around 90% of the fluid critical temperature. Above this value, only gas can be encountered in the reservoir. To achieve controlled dispensing and high repeatable cycles, one needs to be capable of regulating the bubble generation, which enables to operate under controlled pressure fluctuation conditions by the balance of the density fluctuations in the chamber [20]. There are two types of superheated fluid nucleation [19]. Heterogeneous and homogeneous nucleation mechanisms occur when super-heating reaches temperatures close to a critical point. The first happens in the solid or liquid face of the metastable system and depends on the solid/liquid characteristics. On the other hand, homogeneous nucleation is found within the fluid and occurs at a superheat temperature limit due to density fluctuations caused by temperature increase. The most challenging point of nucleation control in bubble jet generators is turned to homogeneous nucleation independence of the heating surface [21].

Besides ink-jet printing purposes, other applications can be found in scientific applications of

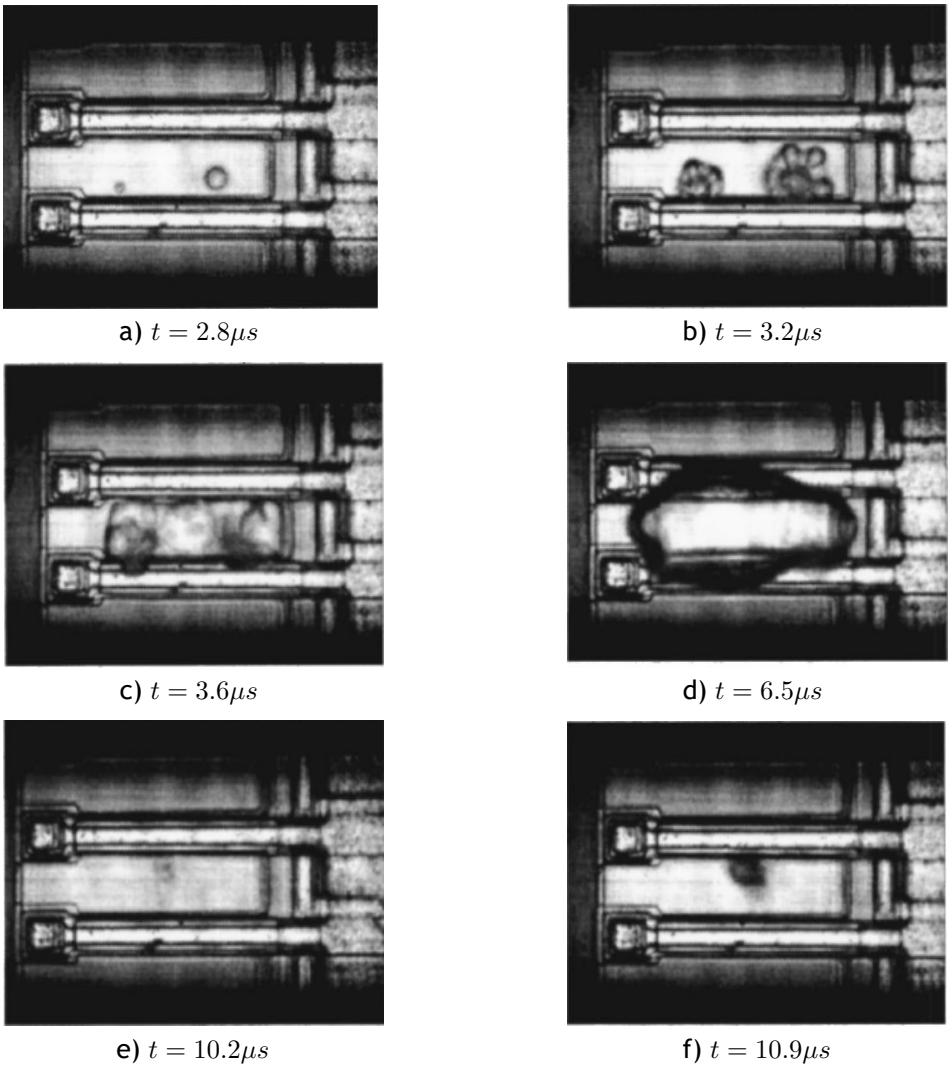

a) $t = 2.8\mu s$ b) $t = 3.2\mu s$

c) $t = 3.6\mu s$ d) $t = 6.5\mu s$

e) $t = 10.2\mu s$ f) $t = 10.9\mu s$

Figure 1.2: Nucleation phases: a) Nucleation initiation; b) Nucleation growth; c) Nuclei coalescence; d) Maximum size of the gas sheet; e) Bubble collapse; f) Refilling of the nozzle [19].

thermal ink-jets. They are noticeable since this type of droplet generators can be employed whenever high precision jetting is required, such as in micro-droplet injection, cytoscribing (cell positioning), and liquid crystal display [16]. In the combustion chamber, bubble jets allow mixing control [22]. Cytoscribing is a field of biomedical science that requires high accuracy droplet dispensing to DNA arraying, which requires high accuracy devices to generate a well defined bio-sheet [23–25]. Its uniform coating capabilities make ink-jet promising devices for flat panel display manufacturing [26, 27].

1.4.2.2 Acoustic Droplet Generators

An inexpensive way of micro-droplet formation is by using a sound source (a loudspeaker or a regular radio speaker connected to an amplifier for example) to create a mechanical disturbance on the membrane. This type of droplet generator consists of an assembly of a loudspeaker, a flexible membrane and a fluid chamber [28]. The sound-induced membrane oscillations caused by the signal originate pressure fluctuations in the meniscus. The pressure increase in the fluid chamber pushes a small portion of the meniscus through the nozzle. The pressure gradient between membrane contraction and relaxation is negative. The phenomenon of negative pressure

gradient causes the meniscus to re-throw into the fluid chamber.

This device can be operated in Drop-on-Demand (Fig. 1.3a) or continuous jet breakup (Fig. 1.3b). the major factor that defines the ejecting process is the flow rate. At a low flow rate, the device is operated in DOD mode and for high flow rates, the device is operated in Stream mode. This droplet generation device is considered a large-scale droplet generator since the actuator is not sufficiently accurate to operate on micro-scale [16, 28].

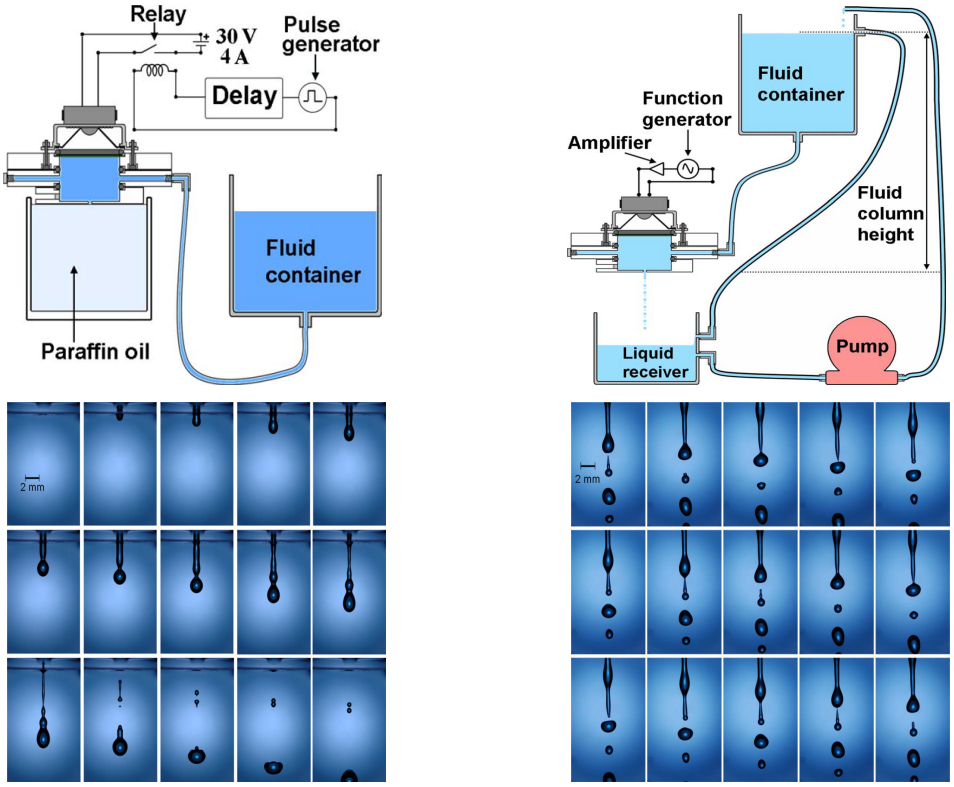

a) b)

Figure 1.3: Acoustic driven droplet generators: a) Drop-on-demand; b) Continuous jet break up [28].

1.4.2.3 Pneumatic Droplet Generators

Pneumatic droplet generators are considered to be another type of MEMS (or NEMS if it is operating in nano-scale) [29]. The principle of pneumatic generators is to apply a liquid or gas pressure in the meniscus by the action of a moving component. Usually, this kind of droplet generators consists of an assembly of a T-junction and a solenoid valve that handles the link of the fluid chamber to the pressurized gas tank as can be seen in figure 1.4. Solenoid valves are a mechanism that uses an electric field to create motion in the pendulum (transforms electric energy in mechanical energy). The solenoid valve is responsible for creating the pressure fluctuations applied in the fluid.

The pendulum movement creates an alternating positive-negative pressure pulse in the droplet generator. In its opened form, the solenoid valve allows the compressed gas to flow into the fluid chamber and pressurize the liquid, pushing it towards the nozzle plane and forcing a portion of fluid through the outlet [30]. Thereafter, the valve is rapidly closed to create a negative pressure pulse to withdraw the fluid back into the reservoir and avoid the formation of a satellite or second droplet.

This kind of droplet generator is frequently used featuring a heater band (represented in figure 1.4 in black) and a temperature controller to generate molten metal droplets [31–33]. In this case, the chamber is heated to a point where the temperature is higher than the melting point of the metal (in this case, the materials used to build the droplet generator need to be heat resistant). Then the process referred above takes place to generate small spheres of molten metals. Engineering frequently uses this technique in circuit arraying or to create small metal particles.

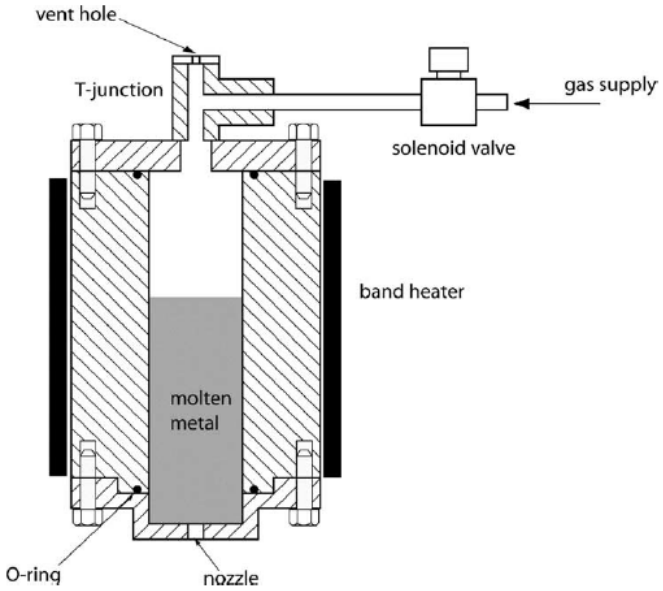

Figure 1.4: Schematic diagram of droplet generator[31].

1.4.2.4 Microfluidic Droplet Generators

The principles behind microfluidic droplet generation use the immiscible characteristics of two or more fluid streams (air and water, for example). The fluid that is to be broken into small droplets is often called a dispersed phase, while the immiscible fluid that involves the droplets is referred to as continuous phase. By colliding the disperse phase stream with the continuous one, the column of the dispersed phase is exposed to a shear force that breaks it into small dispersed droplets. While other ways of droplet generation use an actuator to produce instabilities in a jet or to force single droplets though the nozzle, microfluidic droplet generators use the dimensions and wetting properties of the micro-channels and the flow rate of the fluids [16]. The method is commonly used in emulsions of one or more components [34], since it allows to disperse different components into other fluids, as long as all the phases are immiscible. Microfluidic methods are also used in research fields like generation and investigation of supercooled water and ice nucleation [35]. Microfluidic droplet generation relies upon the interaction of capillary and viscous tensions and the compartments geometry [36]. By simply establishing the flow rate of the different phases in a T-junction or flow focusing (Fig. 1.5) [36], one can produce streams of mono-dispersed droplets.

Using a T-junction configuration, the droplets are obtained by colliding the continuous phase flow (in the main channel) with the dispersed phase [37]. The dispersed phase enters the main channel forming a tongue. The shear forces and pressure gradient, stemming from the continuous phase, create a neck as can be seen in figure 1.5a. The neck gradually squeezes to a point

where eventually creates small droplets of the dispersed phase into the continuous phase [16].

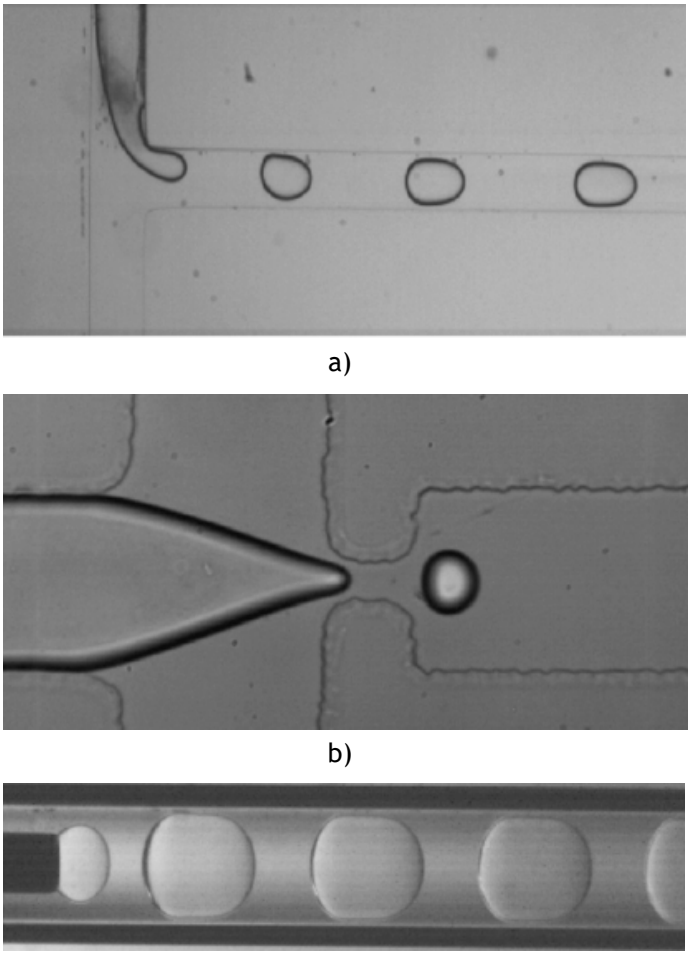

Figure 1.5: Microfluidic droplet generation: a) T-junction configuration; b) Flow focusing configuration; c) Flow focusing configuration with concentric tubes layout [36].

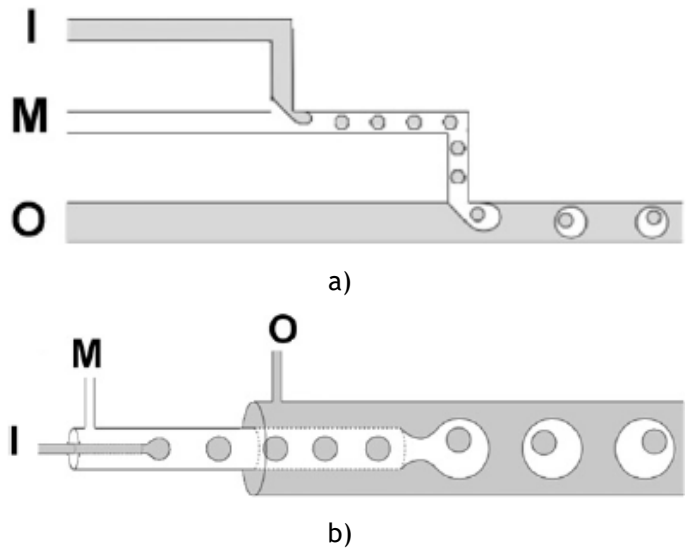

Figure 1.6: Generation of Double emulsions by microfluidic process: a) consecutive T-junction layout; b) two concentric tubes layout [36].

Flow focusing configuration is usually presented in two main layouts: one is operated using two concentric (Fig. 1.5c) tubes, and in the other, the continuous and dispersed phases are forced through a small orifice (Fig. 1.5b). The principle behind the two different layouts is very similar: both fluids have well-defined flow rates and the continuous phase pinches create symmetrical shear forces on the portion of dispersant that eventually breaks into droplets.

In figure 1.5b the dispersant droplet is created by impinging both flow rates and forcing them through a small orifice. The contraction forces shearing of the dispersed phase by the continuous phase, thereafter droplets of the dispersed phase are generated [16]. As seen in figure 1.5c flow-focusing configuration can be operated in a two concentric tubes layout. The principle behind droplet formation in this configuration is similar to the one mentioned above (Fig. 1.5b). Usually by inserting a syringe filled with a fluid in a bath of an immiscible fluid, narrowed by a concentric tube, one can generate micro-droplets with diameters confined by the wall of the bigger tube.

A promising way to employ microfluidic droplet generation to create double emulsions (Fig. 1.6) [36, 38]. The technique enables 100% encapsulation of reactive products. The double emulsion consists of the generation of droplets with smaller droplets inside of them as seen in figure 1.6.

Figure 1.6 presents two different configurations that allow the creation of double emulsion: in a) shows a schematic of the double emulsion employing two consecutive T-junctions and b) displays the same process by the coaxial flow.

1.4.2.5 Electro-Hydrodynamic Droplet Generator

Electro-Hydrodynamic atomization (EHDA) is the given name of the micro-droplet generation process assisted by applying an electric field in a dielectric air-fluid environment. EHDA refers to both the electro-charging of pre-generated droplets and the case where an electric field is applied to assist droplet generation. The present section concerns the latest case.

The principle behind EHDA is based on electrophoresis: when an ionic solution is placed under the effect of an electric field, the system becomes under the influence of Columbic forces between the ionic molecules, moving them in the fluid [39]. The resulting electric force (Eq. 1.6) governs the movement of the particles in the fluid and is given by:

$$F_E = q\vec{E} \quad (1.6)$$

where q corresponds to the charge of the particle and E to the magnitude of the electric field [39]. For this reason, using electro-hydrodynamic assisted droplet generation instead of non-disturbed droplet generation increases the generation rate and reduces droplet diameter, depending on the operation modes [40, 41], which will be mentioned later in this section. As can be seen in equation 1.6, the intensity of the electrostatic force and the magnitude of the applied electric field are proportionally related. Thus by applying a large enough electric, the ions breakthrough a double-layered charged barrier at the interface of the fluid, due to the electrostatic force overcomes the surface tension forces. In figure 1.7 the ejection of fluid through EHD dispensing can be seen. In this image, the dielectric effect can also be analysed.

The electro-hydrodynamic spray depends on the fluid properties and the field strength. This way, by varying parameters like the dielectric constant, electric conductivity, surface tension and viscosity, capillary geometry and the applied electric field, spray generation can be observed

under different spraying modes. By varying the electric field, maintaining the fluid properties, various kinds of electrospray generation can be achieved. The different modes of EHDA are grouped into two big groups: the continuous flow and the discontinuous flow modes. To the latter group belong dripping, micro-dripping, spindle and intermittent cone-jet, while simple-jet, cone-jet and ramified-jet are considered continuous dispensing modes [42].

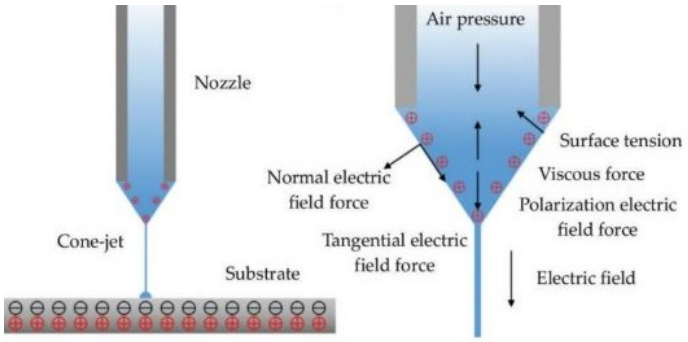

Figure 1.7: Electro-hydrodynamic droplet generator [41].

The dripping mode is achieved by forcing a low flow rate of liquid through the capillary. This droplet generation mode is characterized by generating droplets with a bigger diameter than that of the capillary at low frequency. As mentioned earlier in this section, electro-hydrodynamic assisting this process plays an important role in decreasing the diameter of the droplet and increasing droplet generation [40]. This DOD droplet generation process is usually called electro-hydrodynamic assisted dropping. Micro-dripping is characterized by the observation of droplets with smaller diameters than that of the capillary at a higher frequency than the dripping [39]. The spindle is the mode on which different diameters can be formed. In this mode, the meniscus elongates itself under the form of a jet and breaks into a droplet that can be followed by one or smaller droplets, called satellite droplets. The presence of these droplets is observed when, during the phase when the remaining fluid is withdrawn to the inside of the chamber, the column of fluid breaks into smaller droplets [42]. The intermittent cone-jet mode is characterized by an unstable cone-jet. In this mode, after the cone-jet is formed, it is withdrawn back into the nozzle. During this process, several big sized droplets can be released [42].

When the continuous EHDA modes are issued, there is a continuous ejection of fluid, either by simple-jet, cone-jet or ramified-jet modes. The first two have several similarities, even though they are observed under different conditions of potential. In cases with low conductivity fluids the transition is vague, while, for high conductivity fluids, the transition is sharp and well defined. In the cone-jet mode, the meniscus assumes a conical shape [40].

1.4.2.6 Piezoelectric Droplet Generators

A little over a century ago, the Currie brothers discovered a very interesting capability of some materials. While studying the quartz properties, they discovered that it had piezoelectric characteristics. This lead to the discovery of the first piezoelectric material. The Piezoelectric characteristics define the capability of a determined material to generate electricity when it is subjected to pressure. When a piezoelectric material is compressed, the centre of charge is dislocated. The centre of charge is the average point of the positive or negative charges in a molecule. This way, when the piezoelectric crystal is compressed, the positive centre of charge shifts in one direction and the negative centre of charge in the other. The natural tendency

to match charges allows the extraction of electricity. Latter, the matter concluded that these features were observed due to the presence of molecular polar bonds [43].

Later on, another phenomenon would be discovered: the converse piezoelectric effect [44]. This phenomenon was given this name because it consists of the opposite effect. In this phenomenon, an electric tension is applied to the piezoelectric material, and the material changes its shape. This occurs because the positive pole is going to attract the negatively charged parts of the molecules, and the negative attracts the positive ones. This way, the implementation of an electric tension results on a rearrangement of the crystal molecules. By rearranging the molecules, the shape of the crystal changes, causing it to expand or contract [45].

Piezoelectric droplet generators is the common name used to refer to piezoelectric disturbance assisted dispensers. This is the chosen disturbance source for our device as will be seen in chapter 2. These devices recur to the use of materials with piezoelectric characteristics that implement pressure variations on the fluid chamber or make the outlet section vibrate to generate disturbances into the fluid. The main principle behind this means of droplet breakup is the piezoelectric effect, explained ahead. In piezo-generators, a vibration of the piezoelectric component is induced recurring to an applied electro signal [46]. The vibration is caused by intermittent shape and volume changes of the piezoelectric cell. The disturbance generating process is highly dependant on the characteristics of the piezo-material and signal waveform.

This type of assisted droplet generation devices can be sub-characterized regarding the disturbance source positioning regarding the fluid and other components of the hole device. For these characterizations, the most known are the push, squeeze and shear modes. These three modes can operate in DOD and stream droplet generation. Depending on the characteristics of the device, there might be some that can operate on the two modes, for different working parameters.

For the push mode, usually, the fluid is positioned between the device outlet and the disturbance source [16]. To achieve droplet generation in push mode, the piezoelectric cell usually consists of a diaphragm with a piezoceramic disc. In the disturbance mechanism, the signal is implied on the piezoelectric cell, causing it to change its shape and volume. The volume increase of the piezo-cell makes the volume of the fluid chamber decrease. The decreasing of the volume of the fluid chamber creates a positive pressure differential on the fluid. Increasing fluid pressure causes a portion of the fluid to be pushed through the nozzle. When the piezo cell relaxes, the volume of the fluid chamber increases again, only to cause withdrawing of the fluid. This droplet generator can be used in DOD mode when a punctual disturbance is applied, and in controlled stream jet-breakup when an intermittent periodic waveform is applied. A push mode droplet generator configuration can be seen in figure 1.8a.

Regarding the squeeze mode, the piezoelectric cell is commonly a tube that surrounds the fluid container, squeezing it when excited. In these piezo-generators, the piezoelectric cell is usually a piezoelectric tube wrapped around the fluid chamber. When the piezoelectric cell is excited, its volume increases, squeezing the fluid reservoir. This triggers a chain of events similar to the ones working on push mode. This kind of droplet generators is usually used to create monodisperse jet breakup, but the concept was sometimes applied to generate drop-on-demand. This droplet generator configuration can be seen in figure 1.8c.

As for the shear mode, the vibration is usually implemented directly on the ejecting fluid. The shear mode is one not so easy to machine. The concept behind this kind of droplet generator

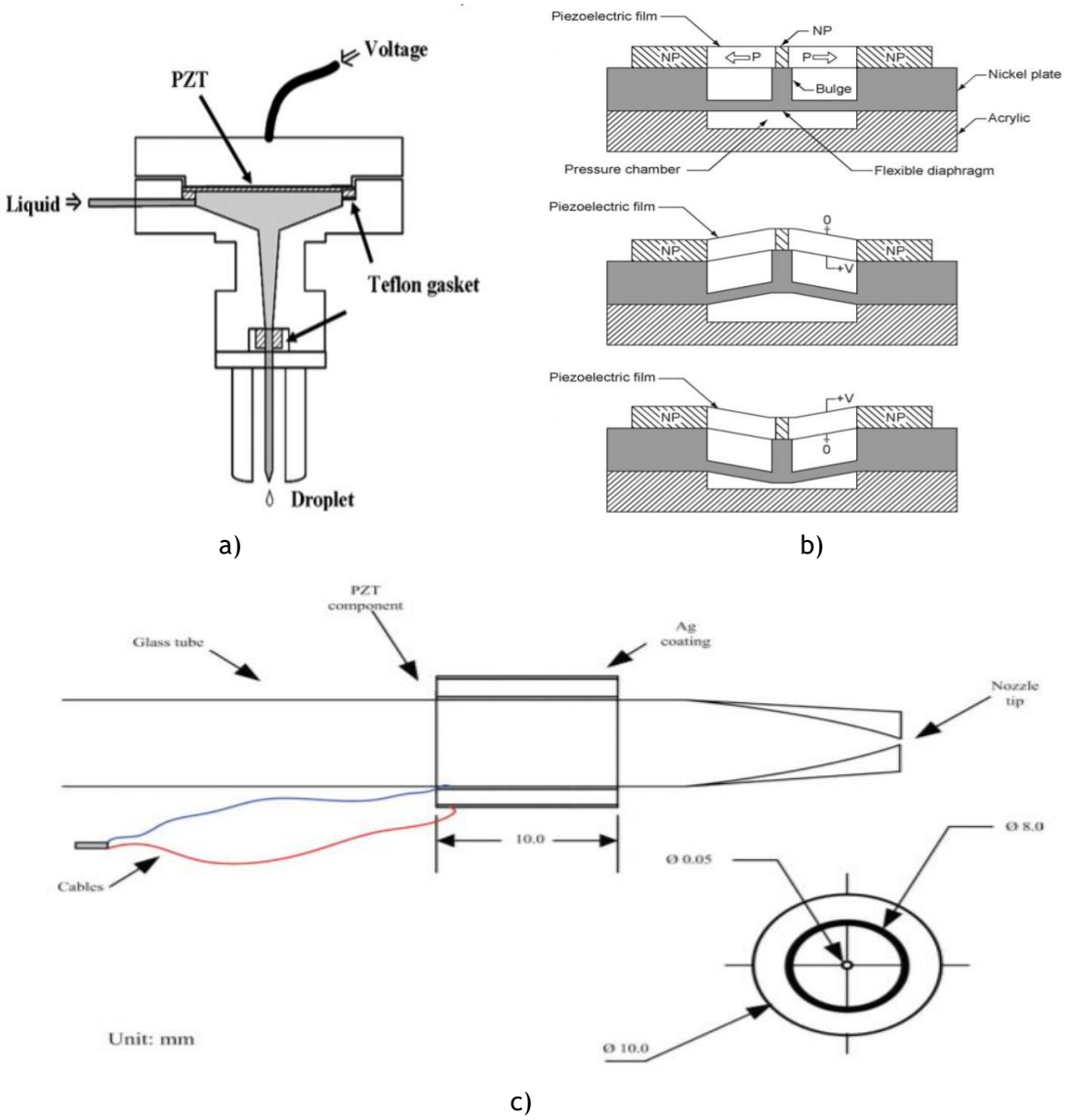

Figure 1.8: Piezoelectric dispensing configurations: a) Push mode [46]; b) Shear mode [47] ; c) Squeeze mode [48].

places the piezoelectric cell at the outlet of the device. In this concept, the flow rate is implied and the nozzle vibrates upon a received waveform [48]. These vibrations are, again, caused by the changes in the volume and shape of the piezoelectric cell, which cause a change of the nozzle shape. Again, this concept can be used to induce early breakup in DOD mode, but sometimes the method is also used in stream breakup, inducing a periodic instability to assist the Rayleigh effect. A diagram for the squeeze mode piezoelectric droplet generator can be seen in figure 1.8b.

Piezoelectric droplet generators present an important role in the dispensing industry. Some of its many advantages are versatility and easy handling. This type of droplet generator presents an affordable alternative to thermoelectric, pneumatic, electro-hydrodynamic droplet generators. This section provides a good contextualization of piezoelectric droplet generator concepts and background. In an initial phase, the piezoelectric effect is briefly explained. Then the different types of piezoelectric droplet generators are shown. Finally, a breve contextualization of past work on this matter.

1.4.3 Background

Lord Rayleigh [14, 15] performed his studies on breakup of undisturbed jets into droplets. He provided a numerical model to predict, what was believed at the time to be the jet breakup behaviour.

Lin [49] designed an built a shear mode stream breakup droplet generator to break up streams of droplets. The concept behind this droplet generator is a vibrating nozzle. With this device, they were able to generate droplets, for which the diameter range from 10 to 100 μm, varying with the applied signal.

Basaran [1] provided a small review of the different droplet generation mechanisms and on droplet generators. Still, on the review side of the droplet generators, Eslamain and Ashgriz [16] published their review on drop-on-demand generators on the "Handbook of atomization and sprays". In the same edition of the journal, Brenn [50] presented the same line of work for droplet generators operated in-stream breakup.

Sergeyev [51] present an inexpensive device capable of generating droplets as small as 17 μm diameter. Through the performed experiments, they were able to operate the device in DOD and stream modes. The presented device was built from a used printer cartridge. The DOD/Stream modes transition is dictated by the applied signal frequency.

Friend and Yeo [**?**] published their investigation on piezoelectric dispensers on the "Encyclopedia of Microfluidics and Nanofluidics" in 2008. Wu [29], in 2007, published their review work on mono-disperse atomizers to apply in Spray drying technology. In this paper, they provide a breve review in droplet generators. With this work, they showed that monodisperse droplet generators can be used for spray drying technology.

Fan [46] designed a DOD push mode generator that recurs to the use of a piezo-diaphragm to implement a disturbance. For this device, they used glass pipettes as a nozzle. They concluded that the device can be used for high accuracy applications.

Hoeve [4] studied the breakup of undisturbed jets under Rayleigh instabilities through high-speed imaging. They compared the results of the experiment with a lubrification approximation model that takes the inertia, surface tension and viscosity into account. Besides the experiment limitations, the one-dimensional model was able to successfully predict the behaviour of the jet breakup. This way, they were able to prove the dependence of the droplets breakup in the velocity and viscosity. They were also able to prove that the secondary droplet formation depends on the same parameters.

Li [52] designed and built a squeeze mode DOD generator that is able to exchange nozzles. Their device possesses the capability to include different nozzles. This apparatus was able to dispense liquids at high velocities with good repeatability.

Wu [48] studied the monodispersity on the formation of streams of droplets from a jet breakup. For this experiment, they used a squeeze mode droplet generator. They concluded that monodispersity can be achieved by squeeze mode droplet generation. They were able to prove that signal frequency and velocity influences the monodispersity and semi-monodispersity phenomena. They were also able to conclude that fluids with higher viscosity possess a wider range of frequencies that produce monodisperse droplets.

Harris [53] present a low-cost design to be operated in drop-on-demand mode. The presented device was able to generate droplets with diameters ranging from 0.5 to 1.4 mm, depending on

the signal implemented on the piezoelectric cell. For this experiment, they were able to obtain 0.5% accuracy on the produced diameters.

Chapter 2

Experimental Procedure

This chapter issues the experimental procedure from the creation of the experimental facilities to the data processing. Initially, the droplet generator is shown. In section 2.1, the droplet generator design, construction and specifications are shown in detail. In order to show the projection process, the different components and designed parts are detailed. Later in the first section, the final assembly of the project device is shown during the project and building processes. Then, in section 2.2, all the additional items used in the experimental facilities are shown and their respective specifications are referred. In section 2.3, the testing process is explained in detail. Thereafter, section 2.4, the data processing and extraction methods are detailed. The extracted data is a means to validate the micro-droplet generator.

2.1 Droplet Generator

In this section, the droplet generation components and respective characteristics are issued. For this purpose, the different constituents of the droplet dispenser, such as disturbance source, nozzle, and design parts are shown in detail. The droplet generated was required to be able to generate controlled size micro-droplets and monodispersed stream of droplets, so the design and characteristics were thought to fit these requirements while enabling to exchange the nozzle diameter.

Initially, a piezoelectric cell is presented as the disturbance source and three stainless steel pinholes with different diameters were purchased to be used as a nozzle. After both these items were chosen the design was thought to fit them as will be shown in the subsection 2.1.3 and 2.1.4.

2.1.1 Disturbance Source

As seen in section 1.4, there are many ways to implement a disturbance in a flow rate into breaking into small droplets, such as thermoelectric, acoustic, pneumatic, piezoelectric, microfluidic and electro-hydrodynamic assisted droplet generators. After deep investigation on the different types transcribed above, the one thought to fulfil the necessities of the present and future investigations were the piezoelectric assisted atomization. Piezoelectric cell operation in a droplet generator depends, as seen in chapter **??**, on the positioning it takes concerning the fluid mass. While piezoelectric tubes are usually operated in squeeze mode and are extremely expensive, when made to customized dimensions, piezoelectric plates are used in push mode and are easier and cheaper.

For the present work, a piezoelectric diaphragm, with the Part Number SMBA27T05PP (Fig. 2.1), was purchased, from Steminc Piezoelectric [54]. The diaphragm consists of a piezoelectric ceramic disc attached to a conductive metallic plate (Fig. 2.1a).

In figure 2.1b, a diagram of the piezoelectric cell is shown, with the following dimensions: D1=27mm, D2=24mm and t=0.5mm.

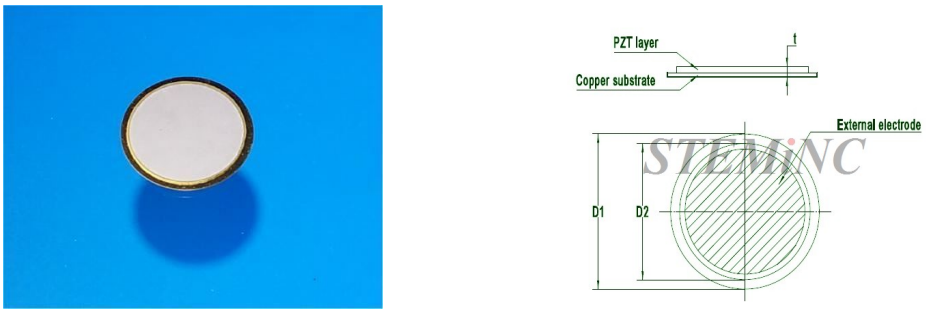

a b

Figure 2.1: Piezoelectric Cell: a) Piezoelectric Diaphragm; b) Diaphragm dimensions diagram [54].

The SM411 piezoceramic disc has 24 mm in diameter, while the copper plate has 27mm. In order to drive the signal from the signal generator to the piezoelectric diaphragm, two copper wires were tined to both the piezo-ceramic and the copper plate, as can be seen in figure 2.2. All the piezoelectric material specifications are presented in the appendix section in table .1.

a) b)

Figure 2.2: Piezoelectric diaphragm: a) front view; b) back view.

2.1.2 Nozzle

In every dispensing system, the nozzle is a very important component to assure the effectiveness of the device. There are multiple types, shapes and sizes of nozzles used when atomization studies are talked about. This project presents a round stainless steel high precision optical pinhole as the nozzle (Fig. 2.3). The accurate part offers a good alternative to needles and are easier to manage. Since one of the requirements for this project is the ability to exchange nozzles, to assure versatility to future works, we acquired three different diameter nozzles (Fig. 2.4), 20, 50 and 100μm, with the respective part numbers #52-869, #36-391 and #36-392, obtained from Edmund Optics on-line [55]. According to the information provided on the manufacturer's website [55], both the 100 and 50μm diameter pinholes have a thickness of 0.03mm, yet the smaller one has 0.01mm.

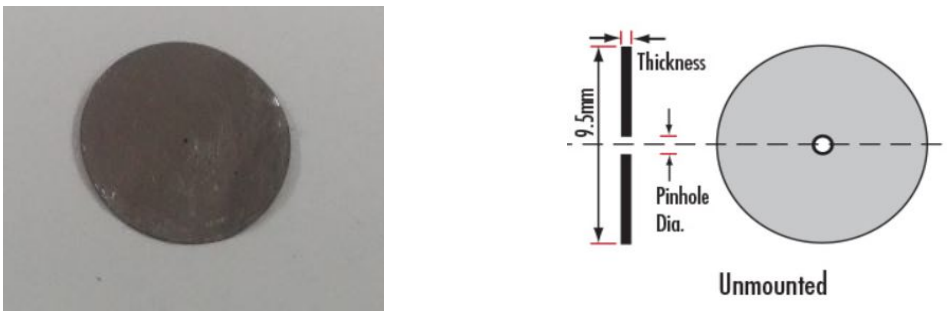

Figure 2.3: Pinhole and Pinhole dimensions diagram[55].

Figure 2.4: 20, 50 and 100μm Pinholes.

2.1.3 Design

As seen in section 1.3, the goal of the present work is to design and build a monosized droplet generator. In this section, all the parts of the design are detailed individually. The dispenser was initially designed in a CAD software CATIA v5, to later be 3D Imprinted. The design is divided into three major parts: lid, body and nozzle holder. The lid part (Fig. 2.6) is the top part of the dispenser, that allows placing the disturbance source (Sec.2.1.1). Body (Fig. 2.7) is considered to be the part that determines the volume of the fluid chamber, and the fluid admission is placed here. The nozzle holder is a two-piece part that enables the enclosure and positioning of the pinhole (Sec. 2.1.2). For this study, the dimensions were set to match the ones of the piezoelectric diaphragm (Sec. 2.1.1) and the pinholes (Sec. 2.1.2).

All parts were designed in CATIA v5 according to the same cross-section, Section 1, shown in figure 2.5. From this initial section, we built different parts of the device.

In figure 2.5 the cross-section used as a base to the construction of the device is shown. This image was acquired from the CATIA v5 R20 software. This section is achieved by combining a circumference of 30mm diameter, in green, with three-holed extension, in white (Fig. 2.5). The holes at the tips have 4mm diameter each to allow the use of bolts and nuts to assemble the different parts as will be shown in the next section.

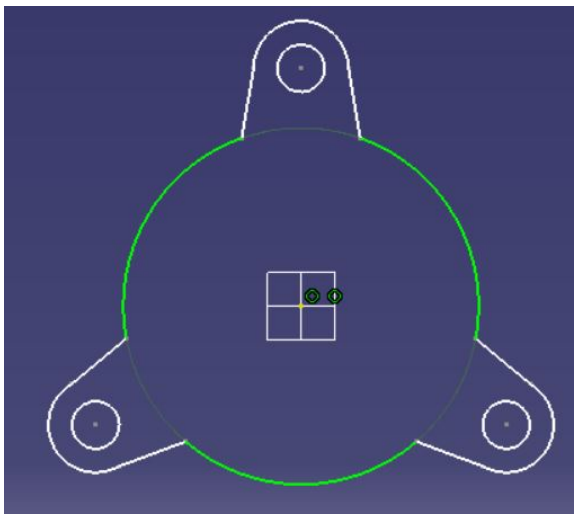

Figure 2.5: Section 1.

The lid was the given name of the top part that confines the piezoelectric diaphragm against the body part (Fig. 2.6). Initially, a flat surface of 3mm thickness was generated from the section shown above (Fig. 2.5). Thereafter, two circular concentric cavities were built: the bigger one has 27mm in diameter and a thickness of 2mm, while the smaller one has a 1.5mm diameter that drills the thinner layer of the existing part, these last features are seen in figure 2.6.

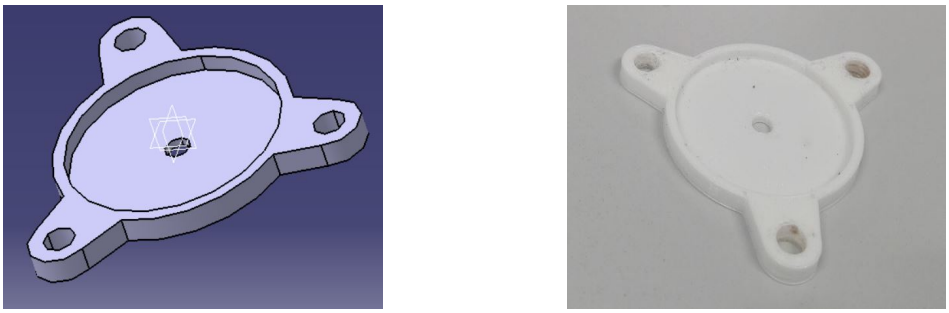

Figure 2.6: Lid part.

Figure 2.6 shows both the CAD design, extracted from the CATIA v5 R20 software and the resulting PLA impression of the lid. The main objective of this component is to fix the disturbance source above the fluid to push the fluid through the nozzle. The small hole allows the electrodes of the piezoelectric cell (Fig. 2.2) to be linked to the signal generator.

The body component (Fig. 2.7) is the compartment that defines the fluid volume in the dispenser device. For the construction of the Body part, the circular part of the design was made and the pins were added afterwards. For the first step, a tube 3mm thick, with a 24 mm inner diameter and 20 mm long, was generated. After this step, the pins were generated on the bottom and top parts of the body. The fluid intake mechanism takes place in this component, as can be seen in figure 2.7. For admission, we used, as mentioned forward in this document (Sec. 2.2.3), a medical tube, in order to drive the fluid to the fluid chamber. In order to make the admission possible, we drilled a 10mm circular hole on one of the sides of the body part.

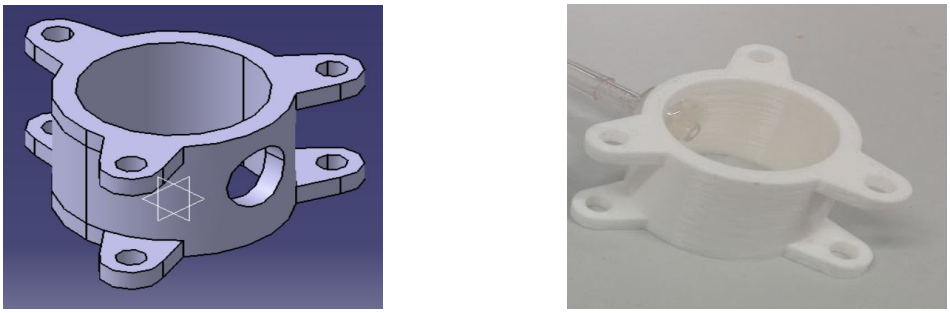

Figure 2.7: Body part.

In figure 2.7, the CAD design, extracted from the CATIA v5 R20 software and the result of the impression of the body are shown respectively.

Placed on the bottom part of the device, two parts compose the pinhole holder, a lid, sometimes referred to as PHL, a base, also referred to as PHB. This set intends to confine and fix the nozzle (pinhole, shown in figure 2.3. In the projection phase, both parts are dependant on the other: the PHB was though in a way to fit the characteristics of the pinhole (Fig. 2.3), and the PHL was thought to fit the pinhole holder base.

The PHL (Fig. 2.8) is the top part of the pinhole holder. This component was conceived from the base geometry, shown in figure 2.5. This part is consists of a plane surface with a 0.8 mm thick protrusion. This extension was projected to fit the pocket on PHB (Fig. 2.9), 9.6 mm in diameter. Thereafter, a concentric drill, of 7.6 mm was added to allow the fluid to arrive at the nozzle. In figure 2.8 the design part can be seen as well as the unmounted part.

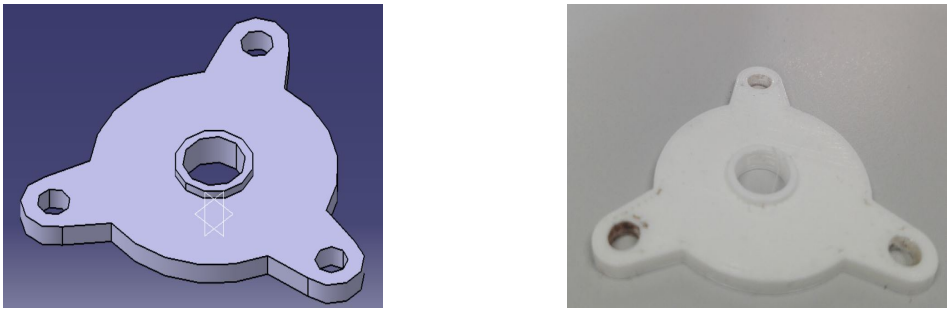

Figure 2.8: Lid of the pinhole holder (PHL).

Figure 2.8 shows the CAD design of the PHL on the left and the part after the 3D impression. As will be seen, forward in this section, this component pressures the pinhole, recurring rubber sealant, against the bottom of the pocket on PHB.

This last part is the one that fits the pinhole in place, assisted by the previous one. The pinhole (Fig. 2.3) dimensions and characteristics are the base of the design of this element since its main function is to secure and protect the pinhole. This part is the junction of a 3mm thick plane surface, generated from the geometry 2.5, and a 1mm thick plane surface, generated from a circle pad made on one of the sides of the first slab, as seen in 2.9. To fit the pinhole, on the top part of this component, a 9.9mm diameter pocket, 2.0mm deep was made as seen in the top pictures on figure 2.9. Afterwards, a tapered hole was made in the second section, clearly seen in the bottom pictures on figure 2.9, to allow the fluid to be ejected.

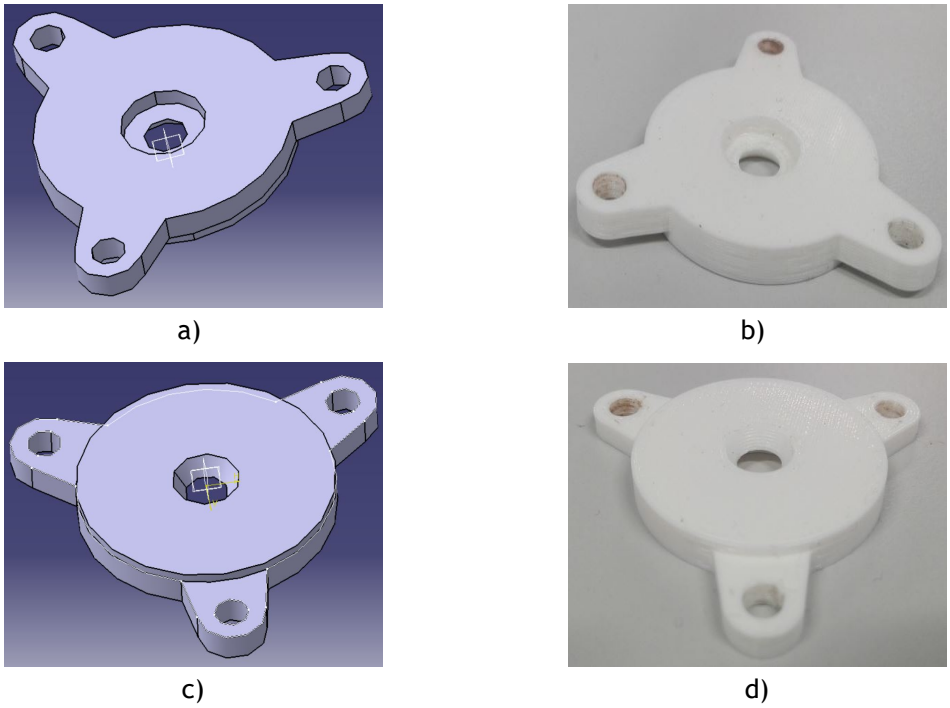

a) b)

c) d)

Figure 2.9: Pinhole holder base (PHB): Top face in a) and b), and bottom face in c) and d).

In figure 2.9, the two pictures on the top show the top face of the PHB, and the two lower pictures show the bottom face of the PHB. When the droplet generator is used as a reference, these faces can be referred to as inner and outer faces respectively.

2.1.4 Final Assembly

In this section, the montage process is detailed. Initially, the tools inherent to the montage are referred. Thereafter, the montage process is detailed step by step. After the design was completed, all the parts were 3D imprinted. With all the parts ready, a medical tube was inserted and glued on the admission hole in the body part, as can be seen in figure 2.10, to allow the fluid to enter the fluid chamber. In addition to the different parts of the design, rubber sealants, washers, screws, and nuts are used. The sealants are made from rubber sheets and are cut to fit the design. Three inter-part sealants were cut from a 1mm thick rubber sheet and two small sealants were cut from a 0.8 thick rubber sheet, to confine the pinhole (Fig. 2.3). The used screws are three 4mm machine screws, with a round head, for the three bottom pins and a slotted drive, and three 6 cm parts of a 4 mm machine screw bar for the top pins. To close the components of the droplet generator together, hex nuts along with flat washers.

Figure 2.10 shows the four parts that compose the final device: PHB on the top to the right, followed by PHL, the body and the lid on the bottom to the right.

The assembling process follows the scheme shown in figure 2.11 and divides into two major sections: the Piezoelectric cell confinement and the pinhole confinement. Both processes are pretty similar since the part joining process is always the same: two or more parts are joined together so that the three pins of each component are coincident with each other, afterwards, the screws are put into the coincident holes, and tighten by the nuts on each screw. In order to prevent breaking of the pins, we used two washers per screw. The parts are joined in the correspondent order, shown in figure 2.11.

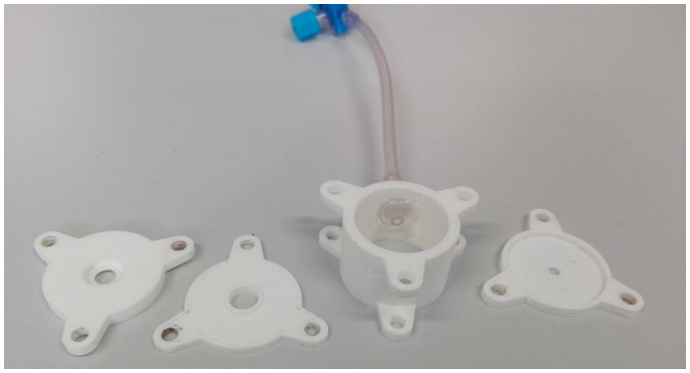

Figure 2.10: Components of the droplet generator.

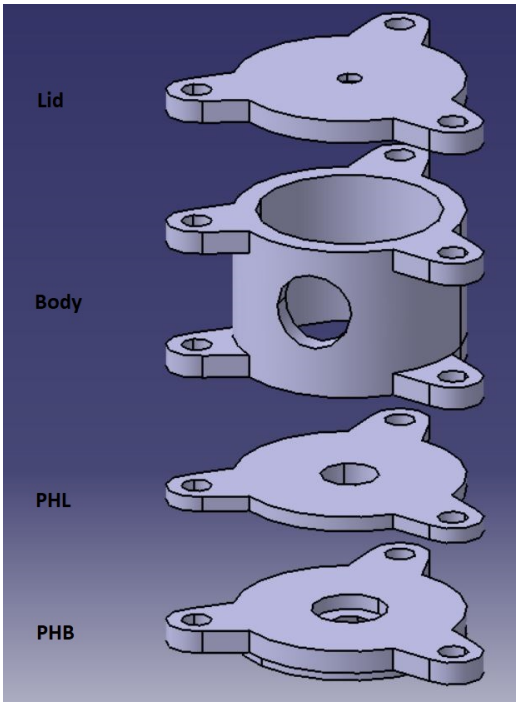

Figure 2.11: Assembly scheme.

In the first step, the piezoelectric cell is confined between the lid and body parts recurring to two of the inter part sealants, passing the electrodes, linked to the metal base, through the hole in the middle of the lid and the one linked to the piezoelectric ceramic through the middle of the holding sealants. First, the piezoelectric cell is placed in the middle of the two holding sealants that seal the compound. After laying the piezoelectric cell between the holding sealants, this small set is confined together by the lid and the body part, after assuring that the piezoceramic is centred on the top section of the body part.

The second step consists of the pinhole confinement. For this step, the pinhole is put on the cavity on the PHB with a sealant on top and one bellow. Afterwards, the PHL part is placed, to secure the pinhole and the sealants. After the pinhole placement, the pinhole holder-pinhole assembly is connected to the body. After these two steps are performed, the device should be able to be operated. Figure 2.12 shows the droplet generator after the assembling of all components.

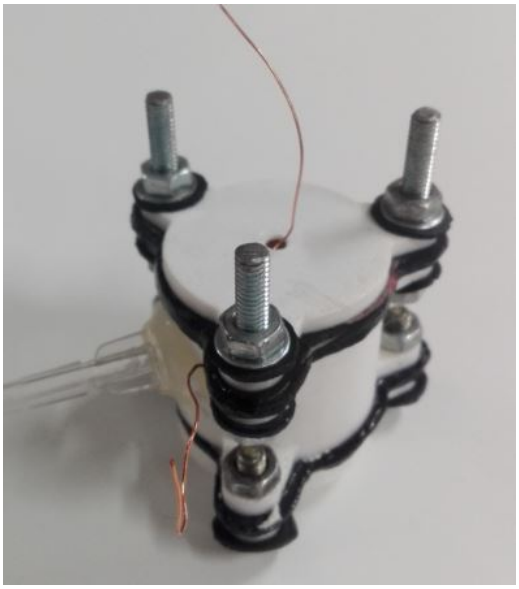

Figure 2.12: Droplet Generator.

2.2 Experimental Arrangement

An experimental arrangement was thought and build to proceed to the validation of the projected dispensing system (Fig. 2.13). The present section issues the different components used in this investigation. The experimental facility can be divided into three principal sections: Image acquisition system, lighting setup and droplet dispensing assembly. All the listed parts are described in detail below. In order to assemble the different components, a table was used to hold all the components as seen in figure 2.13 and a set that involves a glass container, with a squared section of 8 cm, 40 cm high with a blurred surface, and an iron beam, 10 cm long, attached to the droplet generator. Two small wood bars were added, to keep the undisturbed inflow on the feeding tube, keeping the dispensing sight inside the container. The montage of the droplet generator in the support structure is seen in figure 2.14.

Figure 2.13: Experimental arrangement: 1) High speed camera; 2) Droplet generator; 3) Lighting source; 4) Power supply; 5) Signal generator; 6) Syringe pump.

A high-velocity camera (Fig. 2.13 1) used to acquire imaging was placed facing the ejection sight, being manually triggered to capture imaging of different phenomena. To make this possible,

Figure 2.14: Droplet Generator Support Montage.

the lighting source (Fig. 2.13 3) was placed facing the camera though the diffused surface of the fluid container. The fluid dispensing assembly is composed of three major items: a syringe pump (Fig. 2.13 6), a signal generator (Fig. 2.13 5) and the droplet generator (Fig. 2.13 2) issued in section 2.1. Water is forced from the syringe to the fluid chamber through a medical tube, by force exercised by the pump. In order to disturb the generated jet into breaking into droplets, a continuous signal, generated by in the signal generator, is driven to the piezoelectric cell, assisted by the tips of a pico-scope, 2205 A.

2.2.1 Image Acquisition System

Image acquisition is an essential part of the performed study. In order to assure precision, a set of two items, a high-speed camera, with a lens, was used (Fig. 2.15). The camera Photron FASTCAM mini UX 50 was used and presents 1.3 megapixels resolution when working between 2000fps and 60000fps frame rates. Inside the range referred above, image resolution decreases when the frame rate is established at higher values. The lens Macro Lens AT-X AF PRO D was connected to the camera and has the following specifications: 0.3m minimal focus distance,100mm focal length, filter size of 55mm and 1:1 macro ratio. The ensemble is shown in figure 2.15.

Figure 2.15: Photron FASTCAM mini UX 50 and Macro Lens AT-X AF PRO D

The values of time exposure (Shutter) and frame rate were initially set at 1/8192s and 2000fps,

assuming a 1280×1024 resolution as a result, of a diaphragm at 4. The frame rate represents the number of images acquired in a second. Shutter depicts the time the caption is exposed to light, playing a significant role when capturing images of moving objects, since it can significantly improve the final result. After some testing, these parameters were reset to a 2.8 diaphragm, a 1/32768s time exposure and 2500fps frame rate, which resulted in a 1280×800 resolution.

2.2.2 Lighting Setup

Illumination is one important part for testing, for that reason, a LED rope was used and powered recurring to a power supply, as can be seen in the image, as seen in figure 2.16. The power supply alters the energy from an AC to DC mode, providing a uniform distribution of light over time.

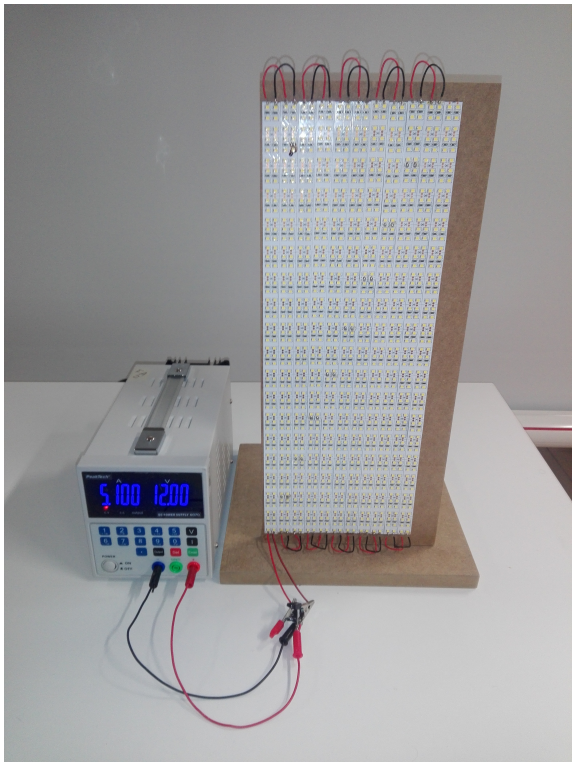

Figure 2.16: Lighting assembly.

The LED rope, was attached to a wood panel and powered by the power supply recurring to a wired crocodile, as shown in figure 2.16. According to the manufacturer, the light source consists of a monocolour adjustable 70w LED ribbon, 12V DC, in the colour cold white. The specifications are listed on .1.

The digital Power supply used was the PeakTech 6070, seen in figure 2.16, that allows the operator to control voltage and current settings. The specifications provided by the manufacturer on the power supply are listed in the appendix section in .1.

2.2.3 Dispensing Assembly

In this section, the dispensing assembly is shown and all its composing components and accessories are detailed. The dispensing system is the group of components that assist in the

droplet formation. This part of the experimental facility divides into three main components: the droplet generator, referred in section 2.1, a syringe pump and a signal generator. The tips of a picoscope and a medical tube are accessories for this part.

Figure 2.17: Syringe Pump NE-1000.

For this experiment, the Syringe pump used was a NE-1000 (Fig. 2.17). This device consists of a 200 per revolution step motor, that provides a maximum force of around 45kg and around 8kg, for minimum and maximum speed respectively. This pump presents a maximum and minimum pumping rate between 6120 ml/hr, for a 60 ml syringe, and 1.459 ml/hr, for a 1 ml syringe, a maximum and minimum speed of 18.36964 cm/min and 0.008409 cm/min. For the present application, a 50 ml syringe was used (Fig. 2.17). A medical tube drives the fluid from the syringe to the fluid chamber. The use of this syringe pump provides high accuracy (1% error) and reproducibility (0.1% error).

Figure 2.18: Signal Generator PeakTech 4115.

Another important part of this droplet generator is the excitement of the piezoceramic. For this, we used the PeakTech 4115 waveform generator, seen in figure 2.18. This device allows us to control the piezoelectric vibration in the fluid compound. For this effect, an electromagnetic wave is generated to excite the piezoelectric cell. With this device, we can control the shape of the wave, frequency, amplitude and other parameters. To drive the waveform to the piezo cell, we used the tips of the picoscope that links the signal generator to the piezoelectric cell.

2.3 Methodology

The experimental testing part is divided into two major parts: a non-disturbed break-up of jets and a second part where the break-up is assisted by an implemented disturbance. The first one has for objective the observation of the non-disturbed jet break up. The second one means to investigate the influence of a piezo-driven disturbance on break up of water jets. For these experiments, all the lights in the room were turned off to provide a dark room, so that the only light source would be the LED panel.

For the first part of the experimental testing, six different flow rates were set on the syringe pump. After the flow rate was established, the device is left running for some time, to assure that the jet is stable when the testing starts. On some occasions, we recurred to absorbent paper to take out the mass of water that was attached to the nozzle. We found out that after this process the jet runs smoothly. After some minutes of running, five testes tests were taken to assure the best result for each case.

After the testing of the non disturbed part of the experiment, the signal generator is set and the picoscope tips are installed to implement the signal on the piezoelectric cell. Choosing three of the previous flow rates, we proceeded to image the ejected fluid. For this part of testing, we used 2.5 ml/min, 4 ml/min and 5 ml/min flow rates. Each of the three chosen flow rates was set and the frequency was gradually increased to find the range of frequencies where the fluid is dispensed in monosized and monodisperse conditions.

To assure that all the jet/droplet plane is in focus, the jet was focused and the testing process was started. In each case, five tests were taken in a row. After the testing of each case, a shot of the background was taken and the dispensing device was removed to proceed to take the sizing reference.

In order to facilitate the identification of the different cases and respective frequency, a nomenclature was created where the numbers refer to a specific flow rate and the letters to a signal form. It is important to mention that the only parameter that was changed in the signal was the frequency in order to analyse the effect on the droplets breakup. The identification of the different cases is shown in table 2.1.

2.4 Experimental Data Processing

2.4.1 Pixel Sizing

In our experiment, all the diameter measurements were made recurring to the image processing, for that reason, pixel sizing is a very important part of these experiments. For every case, a reference was taken to establish the pixel size. For reference, a high precision stainless steel needle was used. The pixel size is then given by comparison with the outer diameter of the needle. The chosen needle has 300μm outer diameter and is seen in figure 2.19.

Recurring to the MATLAB software, a part of code was built to count the number of pixels, on a line, that composes the needle. after the number of pixels is known, it was compared to the outer diameter of the needle. The image processing starts by binarizing the reference image to define the number of pixels that compose the space inside the needle image. The code turns the original image into a binarization of zeros and ones that then result in an image with the black

Table 2.1: Identification of the different cases.

Case -	Flow Rate ml/min	Signal Frequency kHz	Signal Amplitude Vpp
1	2	-	-
2	2.5	-	-
3	3	-	-
4	3.5	-	-
5	4	-	-
6	4.5	-	-
7	5	-	-
2.A	2	3	20
2.B	2	4	20
2.C	2	5	20
2.D	2	6	20
2.E	2	7	20
5.A	4	5	20
5.B	4	6	20
5.C	4	7	20
5.D	4	8	20
7.A	5	3	20
7.B	5	4	20
7.C	5	5	20
7.D	5	6	20
7.E	5	7	20
7.F	5	8	20
7.G	5	9	20
7.H	5	10	20
7.I	5	11	20

and white spectrum, where the white represents the outline of the reference object, shown on the right image of the figure 2.19.

Figure 2.19: Reference and binary gradient.

Thereafter, the code counts, on each line, the number of pixels inside the outline of the needle. Afterwards, the diameter of the needle is divided by the number of pixels in the needle to find out the dimension of the needle. Around ten lines were analyzed to assure accuracy on the pixel sizing.

Even though the camera was kept static for the whole experiment, the working plane could not always be the same, which means that the distance between the camera and the focus plane might not be constant throughout the different cases. For each case, the ejecting device was

kept unmoved throughout the five tests.

2.4.2 Droplets Diameter Extraction

The determination of the diameter of the droplet is a crucial part of these experiments. For this objective, the tested images were processed in order to extract the necessary data. The diameter extraction process is very similar to the one used in section 2.4.1. For the determination of the droplet size, we recurred to the MATLAB software. For this objective, a simple algorithm was developed.

Figure 2.20: Image of the background and dispensed site.

The main code function is the subtraction between the ejection site frame and the background one, shown in figure 2.20. This function, mainly, turns the test image into a matrix of zeros and ones, where the zeros correspond to the empty space and the ones to the stream of droplets. The code then exports the result of the binarization in a black and white image. In the binarization image, the zeros of the matrix are represented in black, and ones in white. The binarization of image is an important tool for the extraction of data since it allowed us to choose the relevant droplets on each frame, that would later be used for the data extraction.

After the main matrix is generated, the number of pixels that correspond to droplets needs to be counted. For that purpose, a second part was added to the code that counts the number of pixels between the first and last frame, on each line of the main matrix, with the representing number 1. This part of the code then gives a vector with all the lines of the image.

Thereafter, the resulting vector was analysed and only the droplets that presented the best approximation between the binarized and original images were used to the final result. From this point on, all the chosen droplets were analysed to give a medium number of pixels the constitute the diameter of the droplet, in each specific case. This method allowed us to predict the associated error of the size of the droplets for the applied conditions. It is important to mention that the maximum number of droplets were analysed from each frame, to assure that the same droplet was not examined more than once.

Chapter 3

Results

This chapter means to validate the proposed design, shown in section 2.1.3, and the overall layout of the components. For that reason, this chapter essentially shows the main result obtained from testing the device. The results of the experiments are divided into three major sections: visualization (Sec. 3.1), effects of the applied flow rate (Sec. 3.2) and signal frequency (Sec. 3.3). The visualization section mainly lists a series of phenomena that were captured during the imaging process, such as coalescence of droplets, jet formation and presence of secondary droplets. Later on this section, the conditions of mono dispersion and monosized breakup are briefly explained and shown. The second section of this chapter issues the effects of the increasing flow rate on the ejection process and droplet formation. Lastly, section 3.3 shows the effects of applying an electromagnetic signal in the piezoelectric cell and the results of varying the signal frequency in the ejection process.

3.1 Visualization

Visualization plays an important role in this project. This section shows the different phenomena that were visualized on these experiments (Fig. 3.1). For that reason, this section is divided into four subsections dedicated to each of the phenomena.

Figure 3.1: Dispensing phenomena.

3.1.1 Jet Formation

In the initial testing, several tests were performed. In this part of the testing, the piezoelectric cell is not excited. The results of the initial testing are shown in figure 3.2. In this initial part, the indicated flow rates were set and the piezoelectric diaphragm was disconnected and free of any vibration, which means that there were no pressure fluctuations in the fluid chamber.

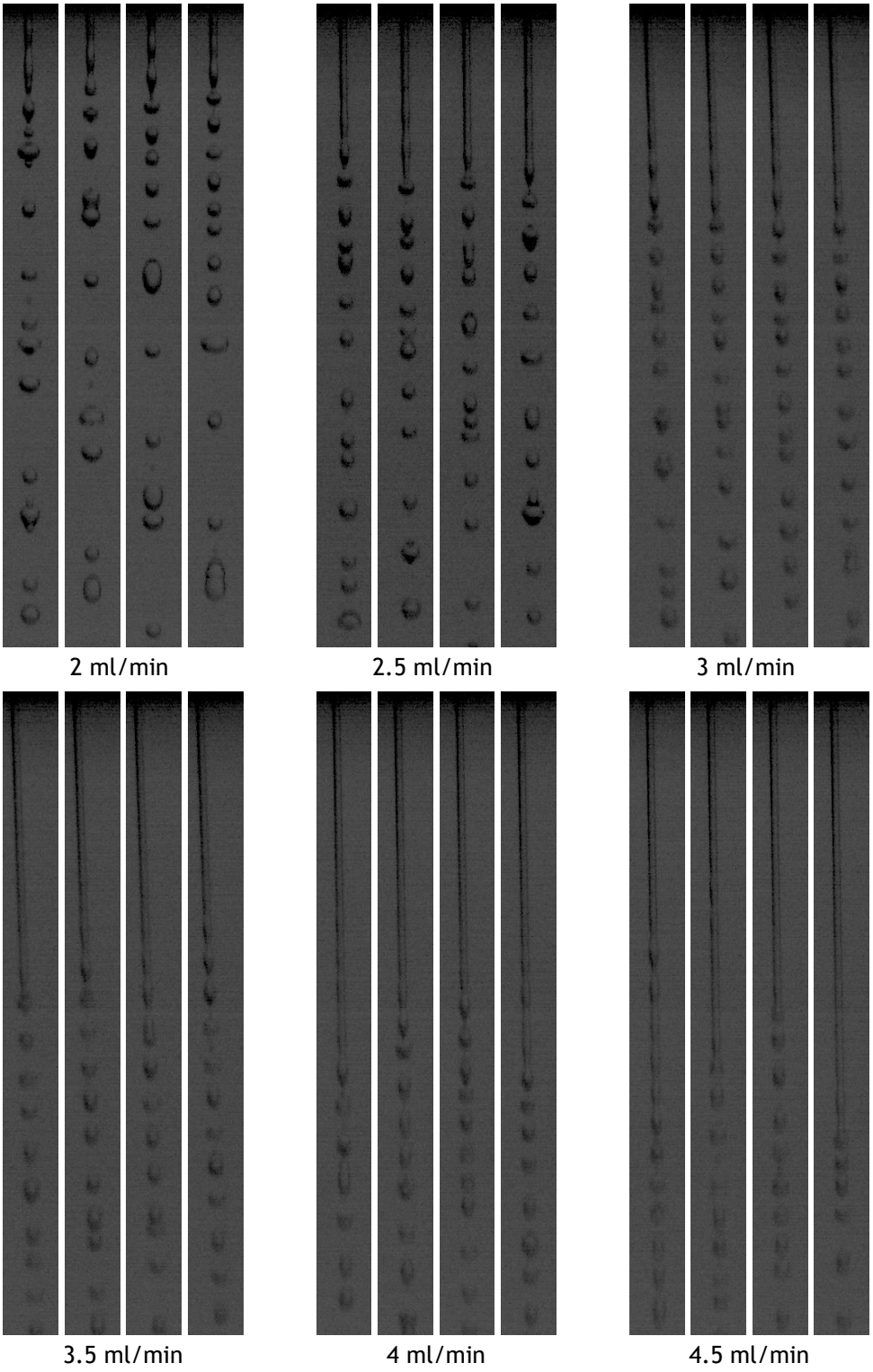

Figure 3.2: Ejection sight of an undisturbed flow rate.

As can be seen, the length of the jet increases with the flow rate. In this phase, imaging was made at 2500 fps and 1/32768 seconds exposure. The shown images were doctored in order to enhance the contrast of the different elements in the pictures. The first case, that corresponds to the to 2 ml/min flow rate was discarded since it showed to be intermittent between dripping and jetting. For this reason, in order to assure the accuracy of the study of the flow rate effect, when the undisturbed testing was repeated, a new flow rate of 5 ml/min was added, that is shown in figure 3.3.

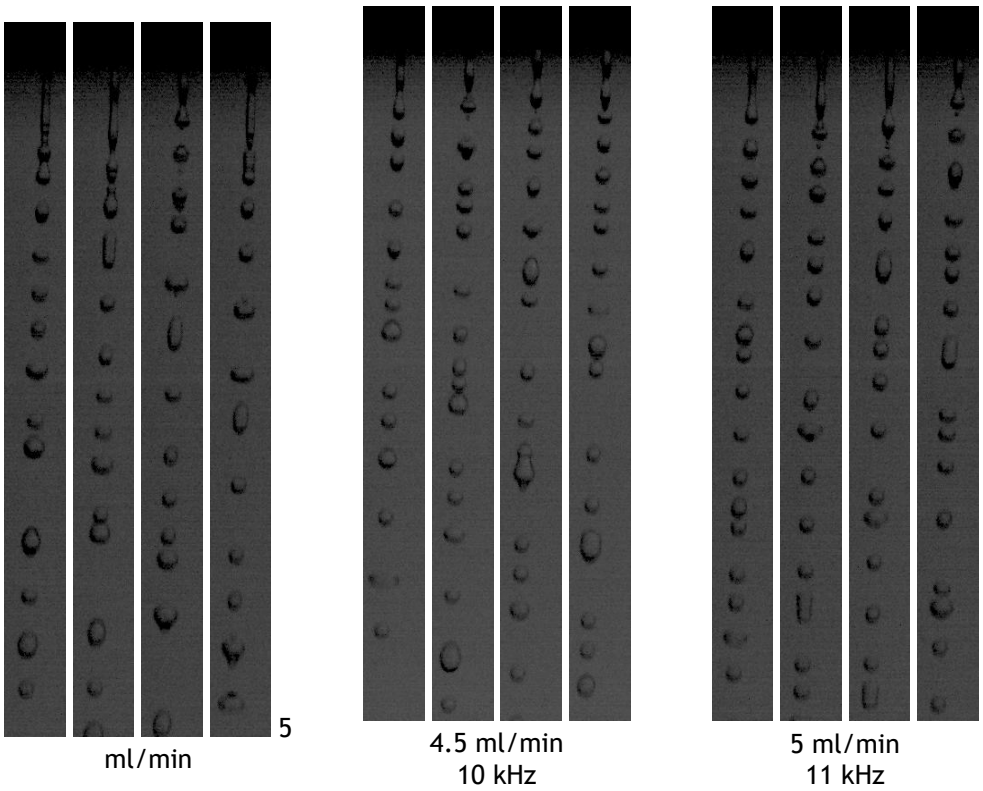

Figure 3.3: Jet formation for the 4.5 ml/min flow rate at 10 kHz and 5 ml/min at undisturbed droplet formation and for 11 kHz signal.

It is important to mention that most of the pictures are slightly altered to improve contrast and legibility. Aside from jet visualization, secondary droplets formation and droplet coalescence are seen in these images and will be studied and explained in sections 3.1.2 and 3.1.3.

Figure 3.2 shows four consecutive frames of the imaging of the different flow rates. In these images, the jets can explicitly be seen increasing with the flow rate.

Besides the undisturbed ejection, the jet formation was also seen for 5 ml/min at 11 kHz signal and for 4.5 ml/min at 10 kHz signal as can be seen in figure 3.3. For both these specific cases, the applied frequencies are a little higher than the monodisperse ejection spectrum of each flow rate. The monodisperse ejection spectrum will be shown later in section 3.1.4.

3.1.2 Secondary Droplets

The formation of secondary droplets happens, as seen in chapter **??**, when a small mass of fluid is released in the form of a small droplet. This happens when the leftover of the fluid withdraws. In some cases, the breakup of one or multiple secondary droplets occurs during the droplet formation process (Fig. 3.4). A secondary droplet is mainly called this way because is generally

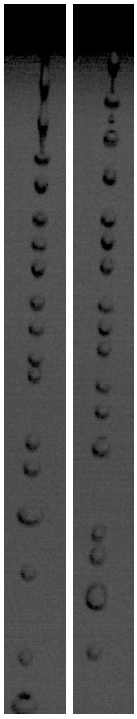

Figure 3.4: Secondary droplets formation.

associated with the formation of another droplet, usually bigger. Some times these secondary droplets join with other masses of fluid, becoming part of a bigger droplet.

In figure 3.4, a case of secondary droplet formation can be seen. The secondary breakup happens after the main droplet is formed. When the main droplet is released, a narrow thread of fluid is left on the pinch of the region (Fig. 3.4). Usually, the thread withdraws to the mass of fluid right above it. In some cases, while the thin portion of the fluid is recalling towards the jet, the fluid thread pinches into a small droplet. This droplet is much smaller than the main droplet. For that reason, they are called secondary droplets and the associated process is called secondary breakup. The phenomenon where the ejection is monodisperse aside from some secondary droplets formation is called semi-monodisperse dispensing.

The phenomenon of the secondary breakup was seen in several testing sights in several cases. Cases like an undisturbed breakup and others that did not make part of the monodispersity spectrum show the formation of secondary droplets. For the 3 ml/min, 4 ml/min, 4.5 ml/min and 5 ml/min the formations of secondary droplets are evident. The secondary breakup study on undisturbed breakup for 2.5 ml/min and 3.5 ml/min flow rates was inconclusive since we could not accurately identify the phenomenon. The high coalescence is the main reason why the result was inconclusive. The secondary breakup was also present on the cases 2.A, 5.A and 7.A. It is noteworthy that similarly to cases 2 and 4, the other cases where coalescence is seen can have non-noticeable secondary droplet formation.

3.1.3 Coalescence of Droplets

Coalescence is the given name of the junction of two or more droplets. If sometimes the coalescence process involves a secondary droplet, it is also called of rebound. This process implicates two neighboring droplets to merge. The process of coalescence can be seen in figure 3.5. In figure 3.5, the presence of secondary droplets, but mainly, multiple coalescence phenomena is

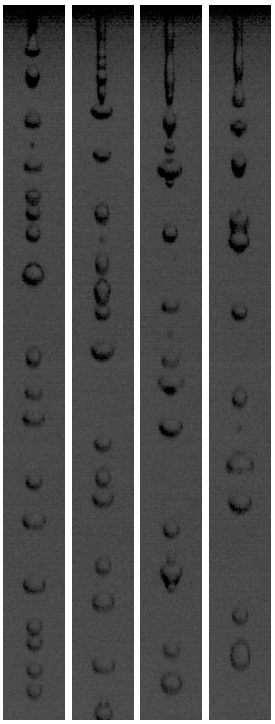

Figure 3.5: Coalescence of multiple droplets.

seen. This phenomenon happens when the two neighbor droplets have different velocity.

The presence of coalescence dictates if the droplet formation is regular or irregular. When coalescence is present, the droplet generation is labelled as irregular. Even though the generated droplets have roughly the same diameter, if coalescence happens, that means that the resulting droplet velocity is not the same on each droplet. This result in coalescence, that originates bigger droplets. For this experiment, coalescence was found in every undisturbed dispensing case, which means that monodispersed dispensing is not met to undisturbed breakup. For the disturbance assisted breakup, coalescence was found for every case except the ones where monodispersity is met. The cases where there was no evidence of coalescence were 2.D, 5.B, 5.C, 7.B, 7.C, 7.D, 7.E, 7.F and 7.G.

In figure 3.5, the progressive coalescence process can be seen. Following the sequence of images on 3.5 from left to right, the progression of some cases of coalescence can be seen. On the first image to the left, a stream of droplets with different sizes and spacing between them. On the second image to the right, an approximation between some of the droplets. The three droplets below the secondary droplets are about to coalesce aggregate. In the image following the last, the two lower droplets, of the three mentioned above, merged together. In the last image, the coalescence of the third droplet of that group to the one previously generated from the merging of the other two. This is a clear case of multiple coalescences.

3.1.4 Monosized Monodispersed Dispensing

This small section focuses on the visualization of the monodispersed ejection, resulting from the performed experiments. Monodispersity, as seen in chapter **??**, is a specific phenomenon of droplet generation. Monodisperse droplet generation was present on every flow rate. The monodispersity is met for specific signal frequencies for each flow rate. This phenomenon

consists of equally spaced droplet formation, with roughly the same size. This phenomenon is usually referred to as optimal stream droplet formation. The frequency of droplet formation is always the same (the droplet formation frequency is the same signal frequency implemented on the piezoelectric cell).

The presence/absence of monodispersity for a determined flow rate and frequency value on a dispensing device dictates its ability to generate streams of droplets in a controlled manner. For the proposed device, we were able to find some points where monosized monodispersed droplet generation is met, the results of the imaging of those cases are shown in figures 3.6 and 3.7. From these images, nine different monodisperse dispensing stages can be seen.

In figure 3.6 one case of monodispersity is shown for a 2.5 ml/min flow rate and two for a 4 ml/min flow rate. The so-called stability happens at 6 kHz frequency value for the first flow rate and between 6 and 7 kHz frequencies for the 4 ml/min flow rate. In figure 3.7, six different cases of monodisperse dispensing are shown. For a 5 ml/min flow rate, the monodisperse dispensing cases range from 4 ml/min up to 9 ml/min. If we look at the images corresponding to case 7.C, it can be seen that the sequence of images seams not to change. This may happen because the applied frame rate is not able to capture the changes. We suspect that the frame rate perfectly aligns with the droplet formation frequency, which means that other frame rated may not capture the same sequence.

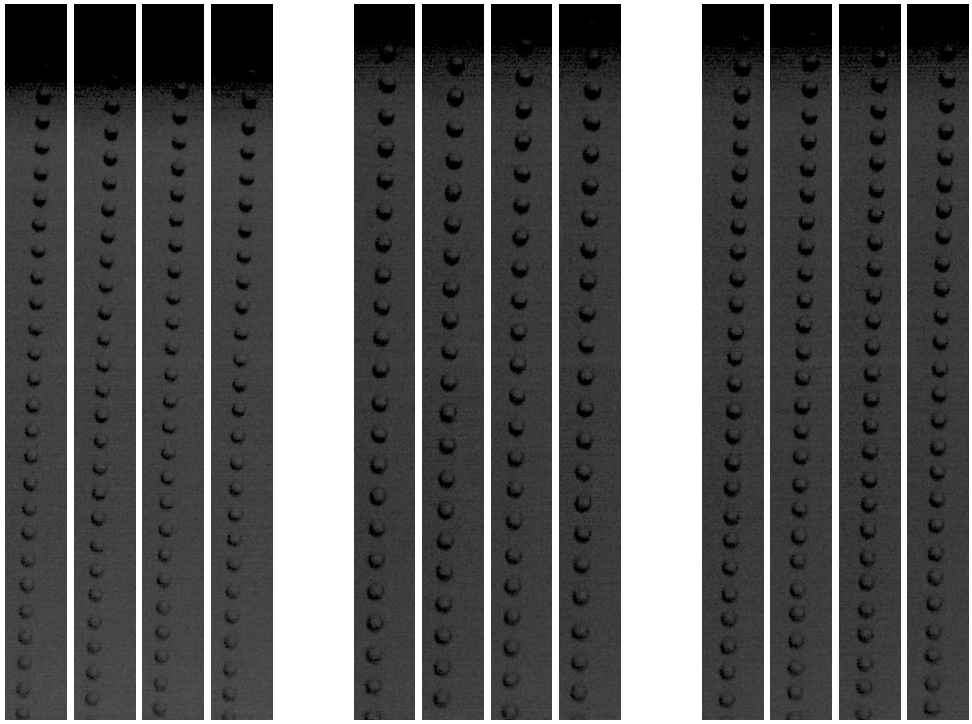

Figure 3.6: Monodispersed dispensing for 2.5 ml/min and 4ml/min flow rates.

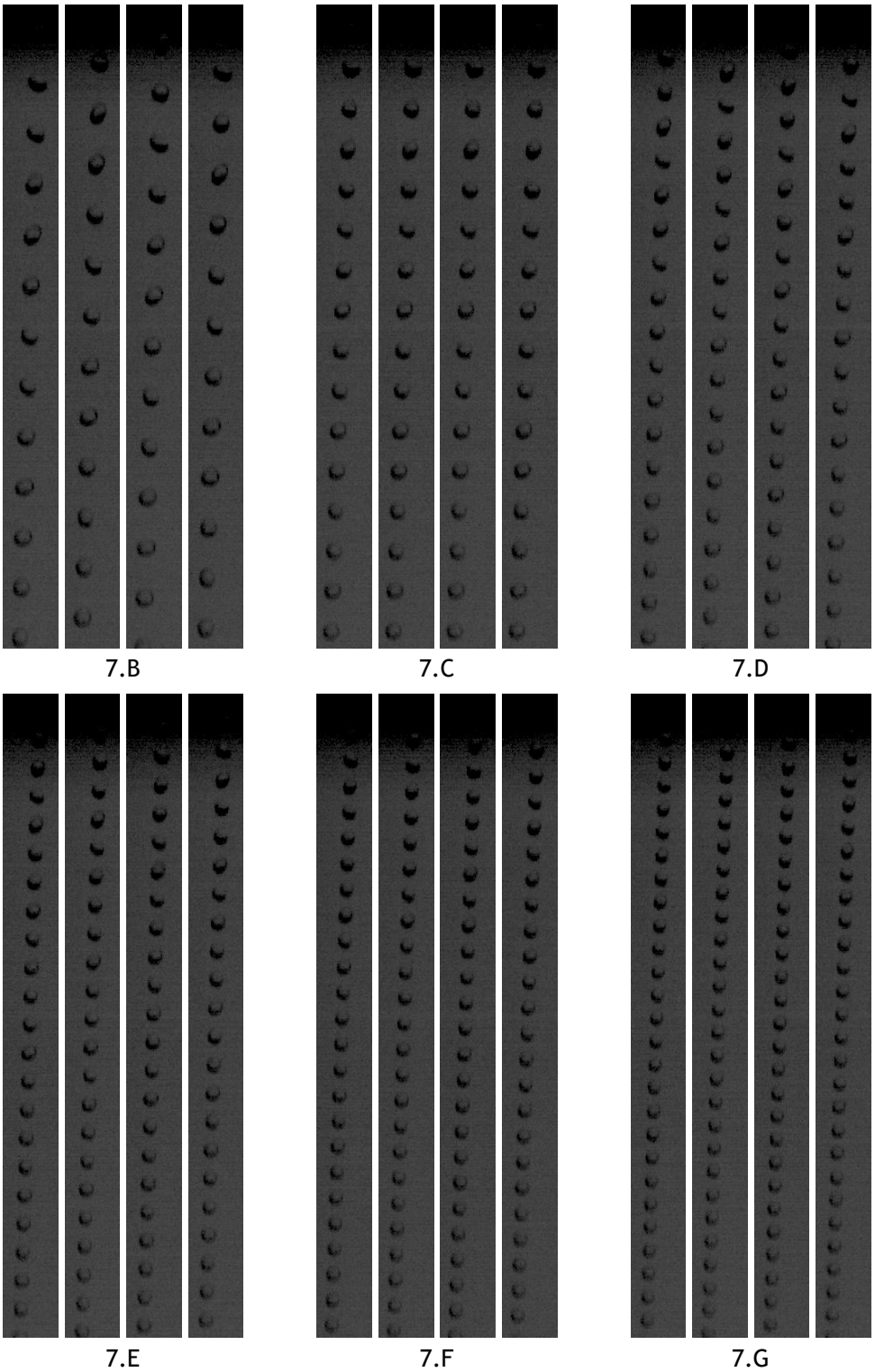

7.B 7.C 7.D

7.E 7.F 7.G

Figure 3.7: Monodispersed droplet generation for 5 ml/min flow rate.

3.2 Influence of Flow Rate in Droplet Formation

In this section, the influence of the applied flow rate on the undisturbed breakup is issued. For this purpose, the diameter of the droplet was analysed, following the steps described previously. The results were gathered and the average value of the diameters of the droplets was calculated.

For this phase, the droplets that resulted from the coalescence of pre-existing droplets were ignored for these studies. The results were then put together in a graph that relates the droplet diameter with the progressively increased flow rate.

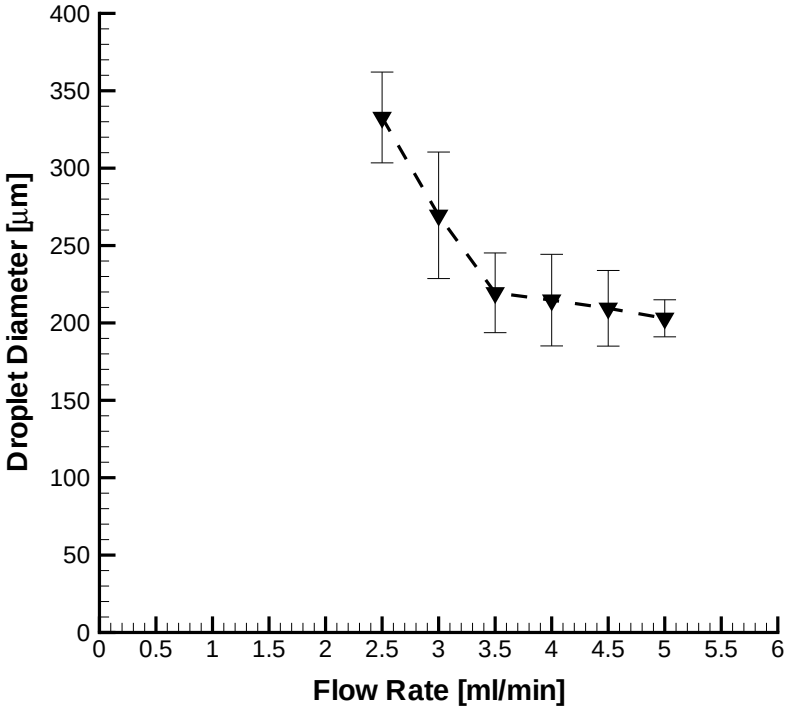

Figure 3.8: Graph: Effect of increasing flow rate on droplet diameter.

Figure 3.8 graphically expresses the progression of breakup behaviour. The major change studied in this phase of the experiments is the dependence between droplet diameter and the applied flow rate. By analyzing the graph it can be seen that the generated droplets diameter falls when the flow rate is increased. From the final results (Fig. 3.8), it can be seen that the results of this study can be approximated by two linear like functions. Between 2.5 and 3.5 ml/min, there is a harsh reduction in the medium droplet diameter. Between 3.5 and 5 ml/min, the graph presents a softer decrease in droplet diameter. For the studied flow rate values, the medium droplet diameter hits its maximum value at 2.5 ml/min flow rate, decreasing with the increasing flow rate, till it reaches its minimum value for the maximum studied flow rate, 5 ml/min.

In the same graph, the standard deviation of each result is also shown. The standard deviation of the droplet diameter is presented in the error bars. These values were used to express the ability/disability, of the device, to generate monosized droplets for each of the flow rates. In this phase of the experiments, standard deviations were found from around 12 μm, for case 7, to 41 μm, in case 3. In this part of the studies, only the generated droplets were accounted for. By ignoring the coalescence resultant droplets, we assure that only the droplets that result directly from the breakup enter for these results. The results of this initial study are shown in table 3.1.

Table 3.1: Droplet diameter for undisturbed breakup.

Case	Flow Rate	Droplet Diameter	Standard Deviation
-	ml/min	μm	μm
2	2.5	332.8	29
3	3	269.5	41
4	3.5	219.5	26
5	4	214.7	30
6	4.5	209.5	24
7	5	203.0	12

3.3 Effect of Signal Frequency

In this second part of the experiment, the effects of the increasing frequency are shown. In this section, different cases will be compared maintaining the set flow rate. For each flow rate, the undisturbed breakup will be compared with the piezoelectric assisted cases. The piezoelectric disturbed cases are also compared between them employing optical and graphical visualization.

As mentioned in section 2.3, for the second part of the studies, three different flow rates were chosen, from the initial part of the work. For this part of the work the flow rates were set and a signal was implemented on the piezoelectric cell to induce its vibration. This section is divided into three main sections, that correspond to a flow rate each, and the final one that aims to compare the overall behaviour of all the studied cases.

It is important to refer that, contrary to the previous section, the coalescence resulting droplets were not disregarded, since the main objective of this section is to find the optimal conditions, for which the device works in monodispersity. The coalescence resulting droplets were not ignored so that we could find a parameter to numerically define the monodispersity cases. It is also important to notice that, for relevance reasons, some cases were not included in the final results of this section.

3.3.1 Effect of Frequency on a 2.5 ml/min Flow Rate

This section is dedicated to studying droplet breakup at increasing signal frequency for a 2.5 ml/min flow rate. This experiment was performed by setting the flow rate at 2.5 ml/min, implementing an electro-signal in the piezoelectric cell at the top of the fluid container. The signal consists of a square function with the maximum amplitude supported by the signal generator, 20 Vpp, and applied frequency was slowly increased. For this specific flow rate, the testing frequencies were increased 2 kHz each test from a base value of 3 kHz to 8 kHz. For this procedure, the base value for the signal frequency was set, tested and increased by 1 kHz. This procedure was repeated until the frequency value was set one or two values higher than the higher frequency where monodispersity was met.

In figure 3.10, the visualization of droplet formation for a 2.5 ml/min flow rate with various signal frequencies can be seen. In case 2.A (Fig. 3.10) the process of droplet formation can be seen for a 3 kHz signal frequency. For this specific case, simply by analyzing this image sequence, one can identify the two phenomena shown in sections 3.1.3 and 3.1.2. Advancing to the case 2.B (4 kHz), tow levels of mono-sized droplet formation were encountered, as well as secondary droplet formation. In case 2.C (5 kHz), the process of droplet breakup seems roughly stable, producing a continuous stream of monosized droplets, however, some coalescence occurrences were observed. By analyzing case 2.D, on the same figure, a stream of roughly monosized and

equally spaced droplets can be seen. For the cases 2.E and 2.F (7 kHz and 8 kHz, respectively), there were no secondary droplet phenomena, but coalescence occurrence prevails these cases.

In figure 3.9, the effect of increasing frequency, for a 2.5 ml/min flow rate, on droplet diameter is graphically shown. This image clearly shows the evolution of the medium droplet diameter with the increasing frequency for this case, where 0 kHz frequency corresponds to the undisturbed case, and 3 and 8 kHz to the minimum and maximum applied frequency disturbance, respectively. From the overall visualization, it can be seen that all the disturbed cases produced smaller diameters than the undisturbed one. When it comes to the disturbed part of this study, an increment of droplet diameter can be seen between the first and second smaller frequencies. From case 2.B (4 kHz) the droplet diameter decreases with the increasing frequency, till it meets its last value for 6 kHz (case 2.D) applied frequency. From this point on, the droplet diameter increases, suffering a more drastic increment between the two higher frequencies.

Still in figure 3.9, the standard deviation of the diameters are shown for each case under the form of error bars. These values were found to be important because they express the capability to repeat the formation of monosized droplets: a high standard deviation corresponds to a low repeatability case and low standard deviation means that the diameters were highly repeatable for the specific case. For these studies, standard deviations were found between 7 and 34 μm. Expressing their values in percentage for each case, the minimum percentage for the standard deviation relating to the droplet size was 3.7% and the maximum was 15% of the droplet diameter. This value can also express the presence of phenomena like coalescence and secondary droplet formation.

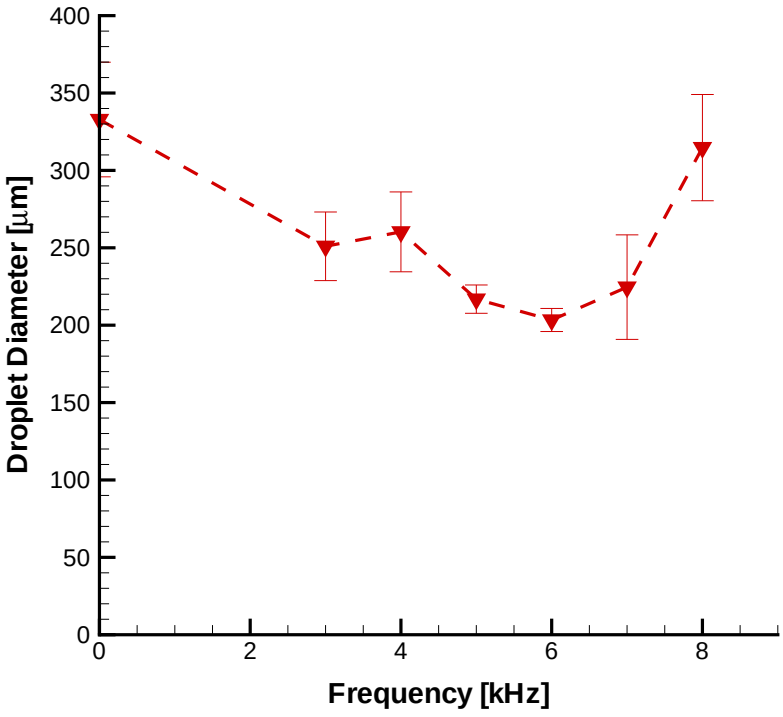

Figure 3.9: Graph: Effect of increasing frequency on droplet breakup, for a 2.5 ml/min flow rate.

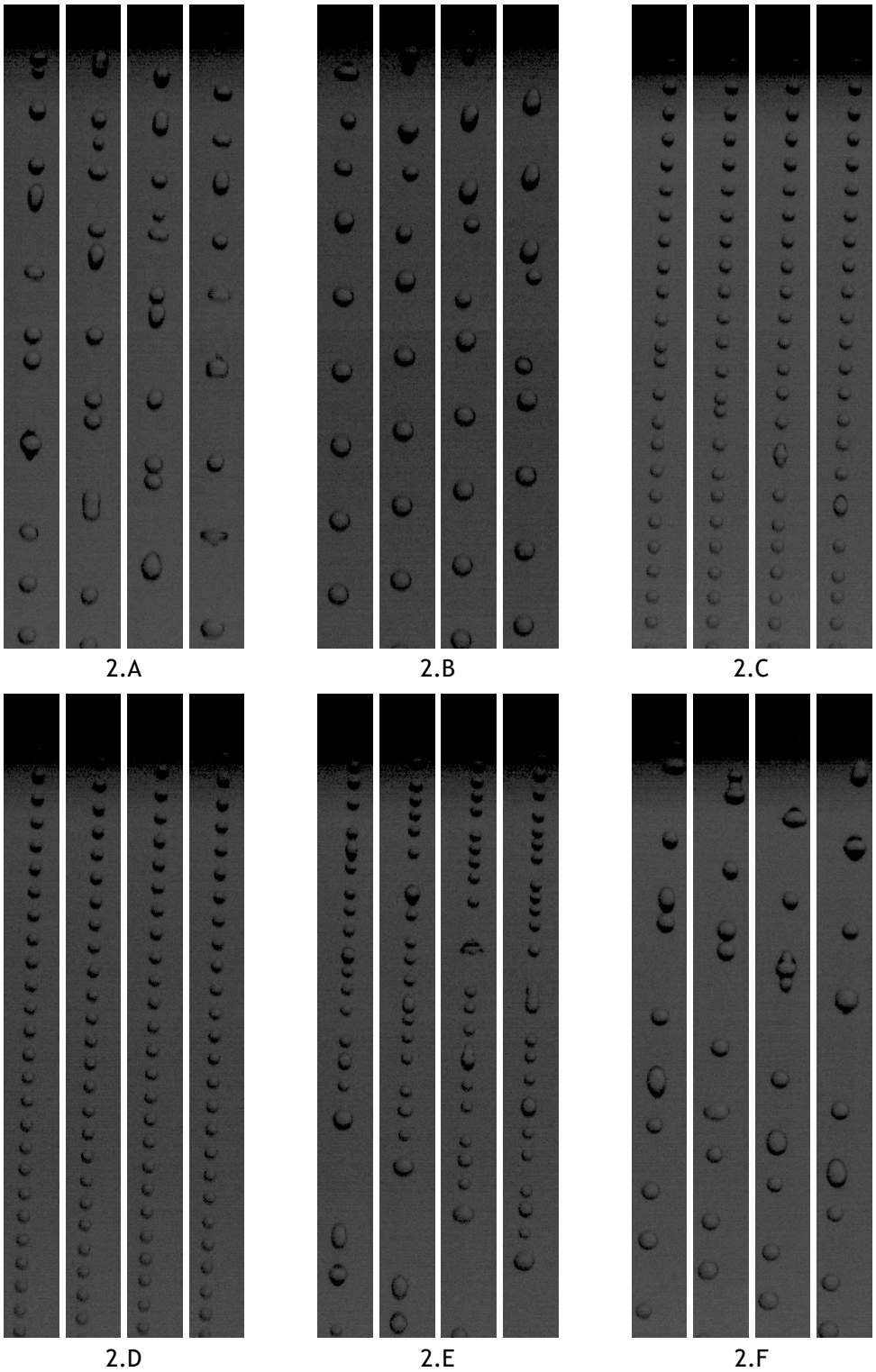

Figure 3.10: Visualization of droplet formation for 2.5 ml/min for increasing signal frequency.

The cases 2.A, 2.B and 2.C show bigger diameters than the ones seen for the cases 2.C, 2.D and 2.E. Also, for both these cases, the generation of multi-sized droplets can be seen. These observations agree with figure 3.9 as far as droplet diameter and diameter variation go. Figure 3.9 clearly confirms the observations obtained from visualization.

From the image sequence of the case 2.D (Fig. 3.10) it can be seen that the variations in the

diameter of the droplet are not significantly high. This observation agrees with the standard deviation seen on figure 3.9. In figure 3.9 it can be seen that the minimum value for the standard deviation stands for the case 2.D. This means that the droplet diameter is kept approximately constant for this specific case. For this motive, this case is listed as one of the monosized droplet generation cases. This point represents the closest case to monodisperse generation and produces droplets of 203 μm.

Case 2.C and case 2.E show the formation of small droplets with some evidences of coalescence. This justifies the closeness of their diameters to the ones in case 2.D. These cases are believed to be a transition between an irregular and regular breakup and vice versa. Case 2.E produces more coalescence than case 2.C. This can also be cooperated by figure 3.9, since the standard deviation for a set 7 kHz frequency is much higher than the one for 5 kHz. Comparing the results of these two cases in figure 3.9 and in figure 3.10, it can be seen that the two methods of identifications of phenomena are cohesive.

3.3.2 Effect of Frequency on a 4 ml/min Flow Rate

This small section shows the results of the studies of increasing signal frequency on a 4 ml/min flow rate. The applied signal is similar to the one in section 3.3.2, it consists of a squared intermittent waveform, with the amplitude set at 20 Vpp, where the applied frequencies are changed. For this experiment, as long as the procedure goes, the approach is the same as in the previous section (Sec. 3.3.1): the flow rate is set (4 ml/min) and the signal frequency was gradually increased, 1 kHz per test, from a base point.

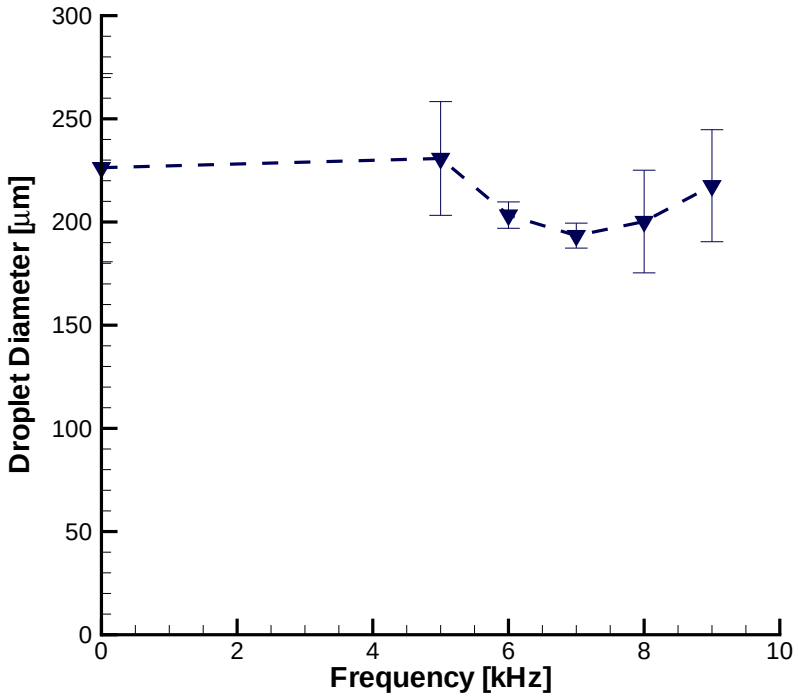

Figure 3.11: Graph: Effect of increasing frequency on droplet breakup, for a 4 ml/min flow rate.

This procedure is repeated until the applied frequency values pass over the monodispersity range. The base frequency value, for this specific flow rate, was set at 5 kHz and went as high as 9 kHz. The results of the test gathering are shown in figure 3.12 and the results of the respective analysis are shown in figure 3.11.

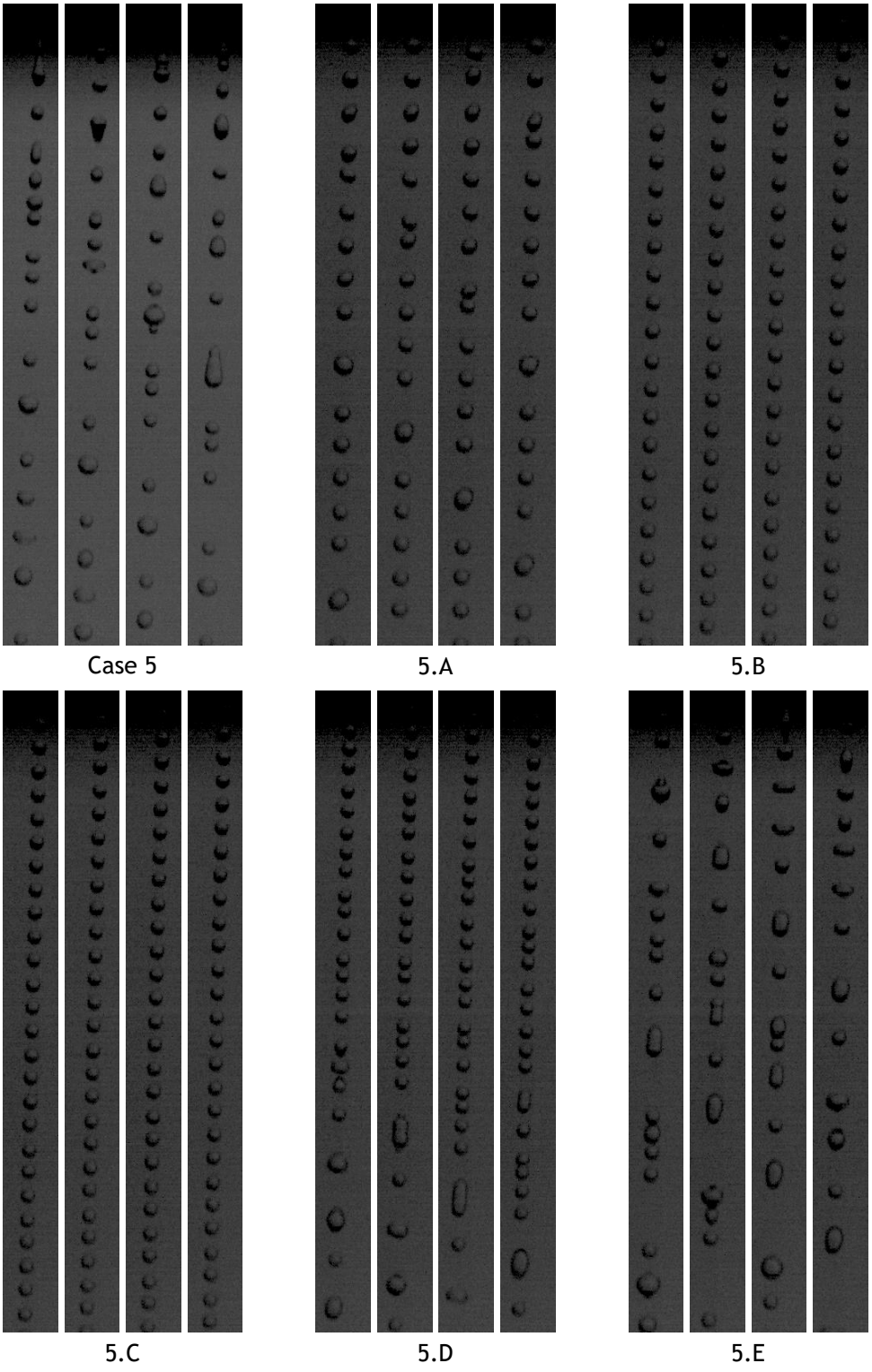

Figure 3.12: Visualization of droplet formation for 4 ml/min for increasing signal frequency.

In figure 3.12, the evolution states of water break up with the increasing signal frequency, for

a 4 ml/min flow rate, are shown. Recurring to visual analysis, the different can be slightly explained and phenomena of secondary droplet formation and coalescence can be clearly pointed out. For case 5, various secondary breakup and coalescence phenomena occurred. The following sequences can be compared side by side since the focus plane is the same. For cases, 5.A, 5.D and 5.E, the two-pointer phenomena of an irregular breakup can be seen (Sections 3.1.2 and 3.1.3). In the cases 5.B and 5.C, consecutive monosized droplet formation can be seen. Comparing the image sequences that correspond to regular breakup, the one with higher frequency value seems to create smaller droplets. This result can not be assured just from visualization, so the images were analysed so the results could be accurate.

In figure 3.11, the graphical representation of the evolution of the diameter of the droplet with the frequency can be seen. This graph compares the undisturbed breakup (0 kHz) of droplets with the piezo-assisted breakup. As will be mentioned further in this document, due to lack of proper illumination, only the diameter of the droplets could be traced. Thereby, the figure expresses the evolution of the generated droplet diameters with the applied frequency. By deeply analyzing the graphical results, it can be seen that departing from the undisturbed breakup to case 5.A, there is a slight increase in droplet diameter. From that point on, the droplet diameter decreases with the increasing frequency until its minimum point, at 7 kHz frequency. From the case 5.C, the values raise until it reaches a value slightly lower than the one produced in 2.A.

Similarly to the cases mentioned in section 3.3.1, for this part of the testing, the capability to generate regular breakup for each case is expressed by the standard deviation. If figure 3.11 is analyzed, high standard deviations are encountered to the majority of the cases. The only cases that present exceptions are the cases 2.B and 2.C for 6 and 7 kHz signal frequency, respectively. In these two cases, the standard deviation present values around 3.1%. These values represent the minimum standard deviations for the study on this flow rate. From the analysis of both figures, two monodisperse generation points are seen for these points, generating droplets with 203 μm and 193 μm respectively. The maximum standard deviations, on this flow rate, were found for the undisturbed breakup case, which presents around 20% standard deviation.

Crossing the information gathered from the visualization of figure 3.12 with the analysis in figure 3.11, the results are cohesive. This means that the numerically extracted values can be corroborated by the breakup visualization. If the visualization disturbance assisted cases are compared with the results in figure 3.11, it can be seen that the two possible regular breakup cases coincide with the ones with the lower standard deviations.

3.3.3 Effect of Frequency on a 5 ml/min Flow Rate

This section is dedicated to showing the results of the investigation of the effects of increasing disturbance frequency, to a set 5 ml/min flow rate. As well as the two cases presented above, the procedure is to set the flow rate and then the applied disturbance frequency is gradually increased. The base disturbance frequency, for this case, was set at 3 kHz and consecutively increased 1 kHz until the frequency range for monodispersity is exceeded. The disturbance signal was a squared waveform with a 20 Vpp amplitude. The applied frequencies are changed. The results are then graphically (Fig. 3.13) and visually (Fig. 3.14 and 3.15).

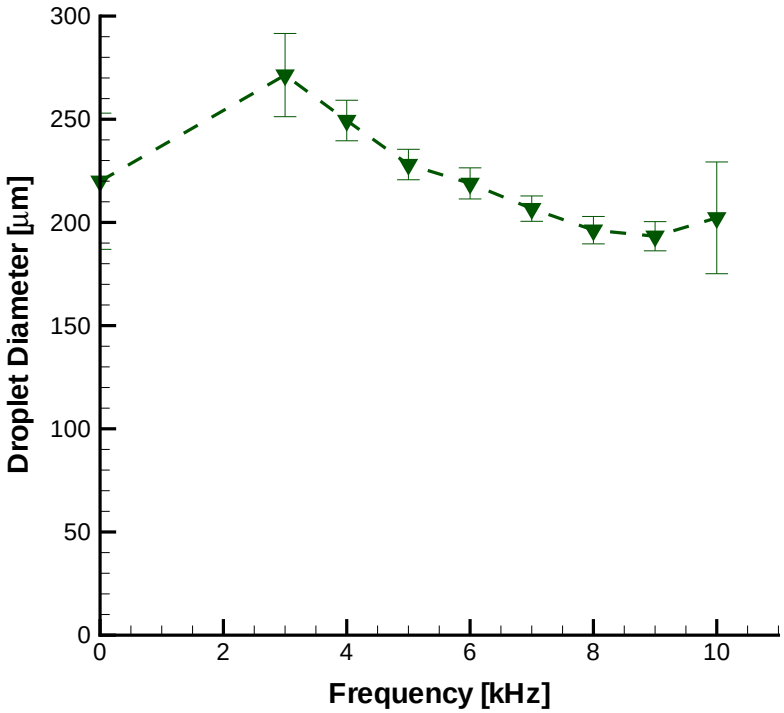

Figure 3.13: Graph: Effect of increasing frequency on droplet breakup, for a 5 ml/min flow rate.

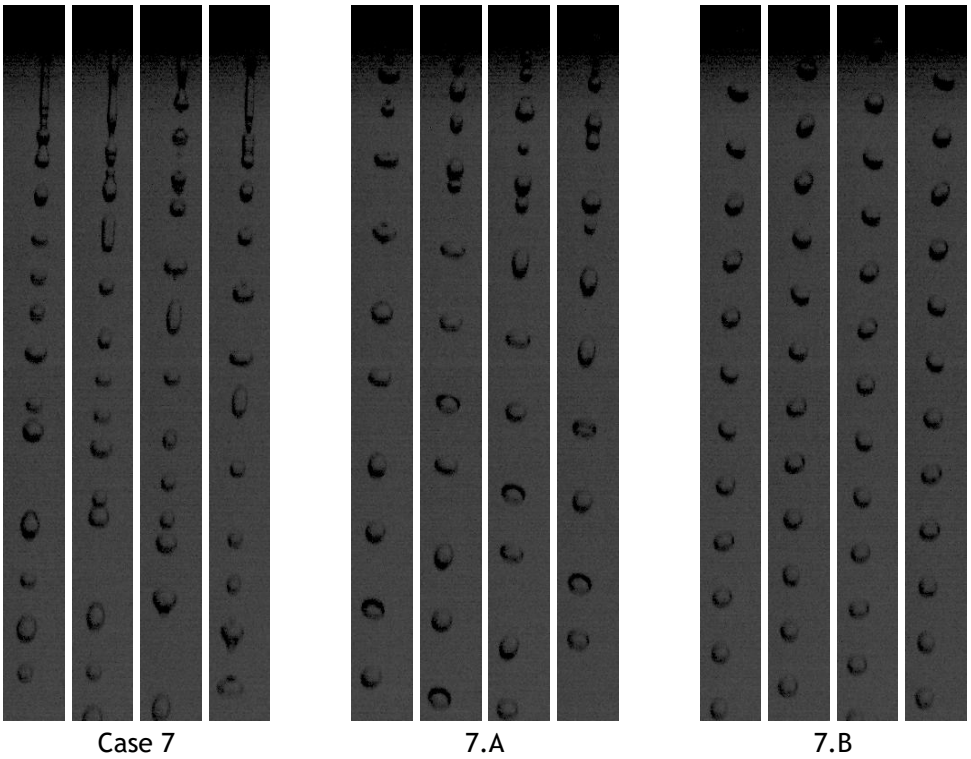

Figure 3.14: Visualization of droplet formation for 5 ml/min for increasing signal frequency.

In figure 3.14, the undisturbed breakup is seen on the left, and the two smaller disturbance cases

are shown. Just by analyzing, the four phenomena shown in section 3.1 can be seen. For Case 7 and 7.A cases, coalescence and secondary breakup are seen. As for case 7.B, what looks like a regular breakup can be seen. Moving on to figure 3.15, the visual presentation of the remaining studied cases can be seen. In figure 3.15, the remaining of the monodispersity frequency range cases can be seen, as well as the one right after this range. Inside the monodisperse range, a decrease of droplet diameter can be seen. From these image sequences, it can also be seen that the spacing between droplets decreases with the increasing frequency.

In figure 3.13, a graphical representation of the evolution of the medium droplet diameter with the increasing frequency is shown, in a 5 ml/min flow rate. By comparing the undisturbed breakup case with the disturbed ones, an increment can be seen in droplet diameter, between the undisturbed breakup and the lower frequency disturbance case. From that point on, a reduction can be seen between the cases until the minimum is reached for the applied 9 kHz frequency disturbance. Between cases, 2.G and 7.H, which presents the higher applied frequency for this study, a slight increment in the droplet diameter can be seen. In the same graph, similarly to the previous cases, the standard deviations of the droplet diameter are presented as error bars. Recurring to these values, the regular breakup cases can be recognized. For this part of the studies, the monodisperse droplet generation could be seen in all the cases between case 2.B and 2.G. By the mathematical analysis, we were able to gather standard deviation lower than 4% of the medium droplet diameter, while on the irregular breakup cases, the standard deviations rose until around 15%. This values corroborated the observations obtained from figures 3.14 and 3.15.

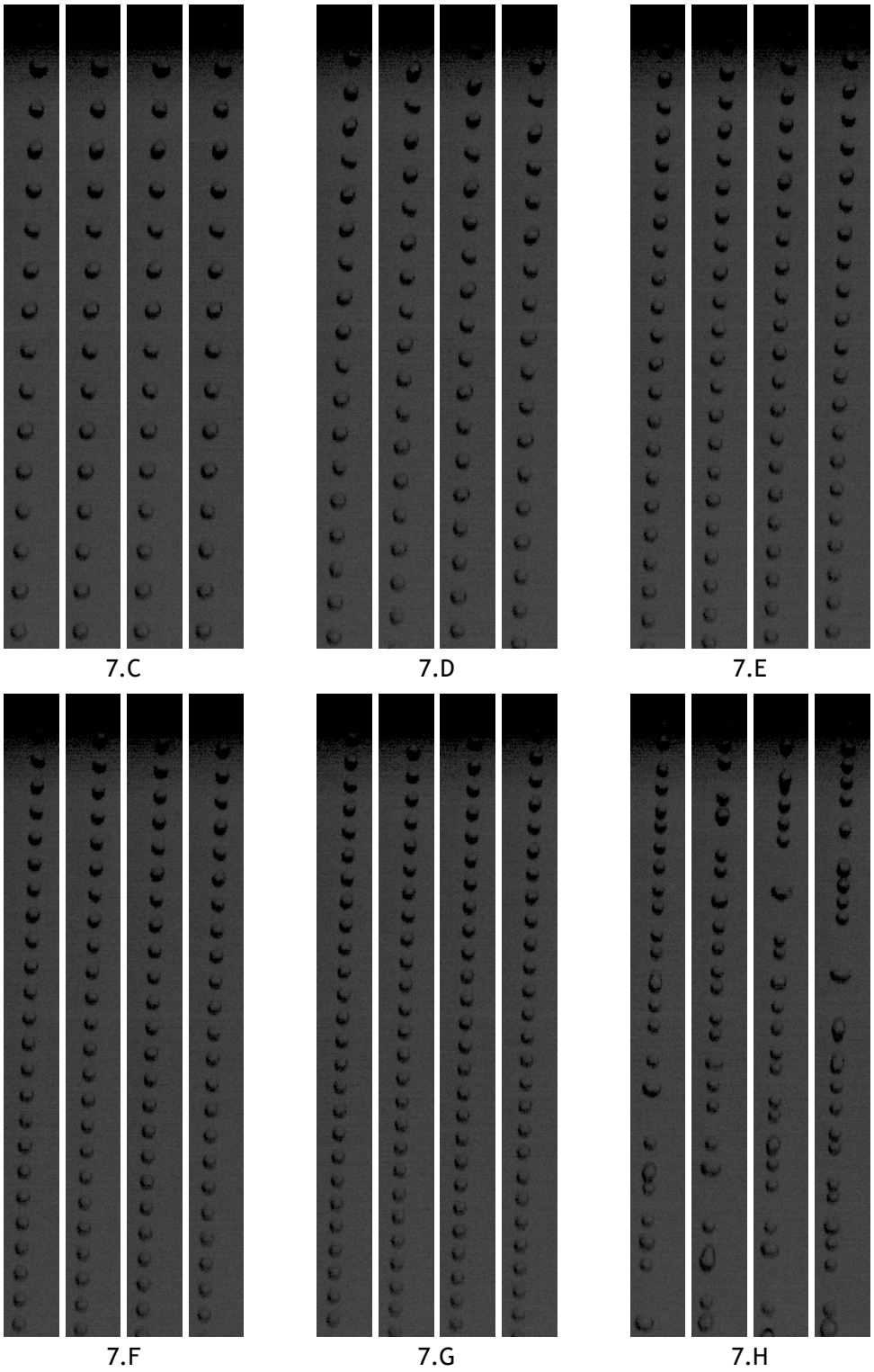

Figure 3.15: Visualization of droplet formation for 5 ml/min for increasing signal frequency.

Chapter 4

Conclusions and Future Work

4.1 Conclusions

Evaluating from the first two chapters, it can be seem that multiple types of disturbance assisted droplet formation have been developed. After deep investigation, we concluded that the best alternative for our case would be to apply a piezoelectric assisted concept to the breakup of droplets. A deep investigation on this kind of droplet generators brought some different configurations to the light set-up. After some consideration regarding advantages and disadvantages of each configuration. After this process, it was decided that a squeeze mode droplet generator offered a good alternative for possible future applications. For the sake of future applications and versatility of the device, we wanted the features of the apparatus to allow it to exchange nozzles.

After that, a new design was developed to respond all of these specifications. As can be seen by the second chapter, squeeze mode droplet generators are usually operated in DOD mode. In this work we were able to create streams of droplets applying a squeeze mode droplet generator. From the testing part of the work, we concluded that the proposed apparatus is able to create streams of droplets in a controlled manner, being able to produce monodispersed streams of monosized droplets for some values of applied frequency.

From the first part of the experiments, nondisturbed droplet generations, we could find out that an increase in flow rate results in the generation of droplets with smaller diameters. From the second set of images in section 3.1, we concluded that the device, under the right circumstances, is able to generate droplets from jet-breakup mechanism. The Formation of droplets by jet breakup could not be recreated.

Advancing to the disturbed droplet generation section of this experiments, several conclusions could be taken from this part. The applied frequency influences the breakup phenomena. The device can indeed work in controlled monodisperse conditions with a well narrow range of droplet diameters. In this phase of the dispensing characteristics, the monodisperse range could be studied, and we were able to conclude that inside the monodisperse spectrum of the disturbed droplet generation, the increasing frequency causes the breakup of droplets to create smaller droplets. This conclusion was obtained by analysing the mathematical graph of the influence of the frequency on droplet breakup for each flow rate, figures 3.9, 3.11 and 3.13. Still from the analysis of these figures, we ascertained that the minimum droplet size generated for each flow rate, corresponds to the bigger applied frequency value in the monodispersity spectrum.

By studying the standard deviations in the monodisperse cases, we can see that the sizes of the generated droplets are highly repeatable for each case. By comparing the three graphs, we were able to conclude that the monodisperse range is wider to higher flow rates.

An important feature of the stream droplet generation is the velocity of the generated droplets

immediately after formation. Although we were able to recall relatively good imaging, we were not able to use them to calculate the experimental velocities. This issue emerged mainly due to the lack of light intensity. To assure an accurate velocity extraction, the frame rate had to be drastically increased, so that the time between frames would be smaller than the droplet formation time. Although a solution was found, another issue arose with this solution regarding the lighting. When the frame rate is increased, our lighting set up did not provide the proper light to assure the needed contrast.

4.2 Future Work

Given the difficulties encountered in this work, a list of different tasks arise to be performed in future works. For future work regarding the project of the device, it is imperative to improve the device when it comes to isolation. Better isolation can allow the formation of new phenomena and improve the overall results in several applications. Another improvement needed for the validation of the device regards the lighting set-up. Improving light intensity would allow the use of higher frame rates without jeopardizing the contrast of the images. Another interesting work would be to experiment with a hydrophobic nozzle. To test if the device can be operated in DOD mode.

After the device is completed, an infinity of applications can be a destination for the apparatus. In my opinion, it would be nice to study the influence of signal amplitude and waveform. It would also be important to customize the apparatus, material-wise so that it can operate with highly corrosive materials like fuels.

There is an infinity of possibilities in investigation applications, such as:

- Application of the device on the fundamental study of the behaviour of fuel droplets upon impact;
- Investigate the effect of micro-size fuel droplets in the combustion process, in aeronautical applications;
- Study the collision droplets;
- Apply the device for studies of multiple consecutive droplets impinging on a dried surface;
- The influence of the impact of consecutive droplets on Splash parameters.

Bibliography

[1] O. A. Basaran, "Small-scale free surface flows with breakup: Drop formation and emerging applications," *AIChE Journal*, vol. 48, no. 9, pp. 1842–1848, 2002.

[2] B. J. Meister and G. F. Scheele, "Drop formation from cylindrical jets in immiscible liquid systems," *AIChE Journal*, vol. 15, no. 5, pp. 700–706, 1969.

[3] C. Clanet and J. C. Lasheras, "Transition from dripping to jetting," *Journal of fluid mechanics*, vol. 383, pp. 307–326, 1999.

[4] W. van Hoeve, S. Gekle, J. H. Snoeijer, M. Versluis, M. P. Brenner, and D. Lohse, "Breakup of diminutive rayleigh jets," *Physics of fluids*, vol. 22, no. 12, pp. 122 003–I;122 003–II, 2010.

[5] B. J. Meister and G. F. Scheele, "Prediction of jet length in immiscible liquid systems," *AIChE Journal*, vol. 15, no. 5, pp. 689–699, 1969.

[6] D. H. Peregrine, G. Shoker, and A. Symon, "The bifurcation of liquid bridges," *Journal of Fluid Mechanics*, vol. 212, pp. 25–39, 1990.

[7] X. Shi, M. P. Brenner, and S. R. Nagel, "A cascade of structure in a drop falling from a faucet," *Science*, vol. 265, no. 5169, pp. 219–222, 1994.

[8] X. Zhang and O. A. Basaran, "An experimental study of dynamics of drop formation," *Physics of fluids*, vol. 7, no. 6, pp. 1184–1203, 1995.

[9] X. Zhang, "Dynamics of growth and breakup of viscous pendant drops into air," *Journal of colloid and interface science*, vol. 212, no. 1, pp. 107–122, 1999.

[10] J. R. Richards, A. N. Beris, and A. M. Lenhoff, "Drop formation in liquid–liquid systems before and after jetting," *Physics of fluids*, vol. 7, no. 11, pp. 2617–2630, 1995.

[11] J. Sartorelli, W. Gonçalves, and R. Pinto, "Crisis and intermittence in a leaky-faucet experiment," *Physical Review E*, vol. 49, no. 5, pp. 3963–3975, 1994.

[12] T. Tate, "Xxx. on the magnitude of a drop of liquid formed under different circumstances," *The London, Edinburgh, and Dublin Philosophical Magazine and Journal of Science*, vol. 27, no. 181, pp. 176–180, 1864.

[13] B. Ambravaneswaran, H. J. Subramani, S. D. Phillips, and O. A. Basaran, "Dripping-jetting transitions in a dripping faucet," *Physical review letters*, vol. 93, no. 3, pp. 034 501–1;034 501–4, 2004.

[14] L. Rayleigh, "Xvi. on the instability of a cylinder of viscous liquid under capillary force," *The London, Edinburgh, and Dublin Philosophical Magazine and Journal of Science*, vol. 34, no. 207, pp. 145–154, 1892.

[15] ——, "On the instability of jets," *Proceedings of the London mathematical society*, vol. 1, no. 1, pp. 4–13, 1878.

[16] M. Eslamian and N. Ashgriz, "Drop-on-demand drop generators," in *Handbook of Atomization and Sprays*, N. Ashgriz, Ed. Springer, 2011, ch. 25, pp. 581–601.

[17] E. Lee, "Microdrop generation (nano-and microscience, engineering, technology and medicine)," 2003.

[18] J. Eggers and E. Villermaux, "Physics of liquid jets," *Reports on progress in physics*, vol. 71, no. 3, pp. 036 601–036 680, 2008.

[19] Y. Hong, N. Ashgriz, and J. Andrews, "Experimental study of bubble dynamics on a micro heater induced by pulse heating," *Journal of heat transfer*, vol. 126, no. 2, pp. 259–271, 2004.

[20] A. Asai, "Application of the nucleation theory to the design of bubble jet printers," *Japanese Journal of Applied Physics*, vol. 28, no. 5R, pp. 909–915, 1989.

[21] R. R. Allen, "Thermodynamics and hydrodynamics of thermal ink jets," *HP Journal*, pp. 21–27, 1985.

[22] S. Baik, J. Blanchard, and M. Corradini, "Development of micro-diesel injector nozzles via mems technology and effects on spray characteristics," *SAE Transactions*, pp. 381–388, 2001.

[23] R. J. Klebe, "Cytoscribing: a method for micropositioning cells and the construction of two-and three-dimensional synthetic tissues," *Experimental cell research*, vol. 179, no. 2, pp. 362–373, 1988.

[24] T. Goldmann and J. S. Gonzalez, "Dna-printing: utilization of a standard inkjet printer for the transfer of nucleic acids to solid supports," *Journal of Biochemical and Biophysical Methods*, vol. 42, no. 3, pp. 105–110, 2000.

[25] C. Maier, S. Wiesche, and E. P. Hofer, "Impact of microdrops on solid surfaces for dna-synthesis," in *Proceedings of the 2000 international conference on modeling and simulation of microsystems*, 2000, pp. 586–589.

[26] D. J. Hayes, W. R. Cox, and M. E. Grove, "Low-cost display assembly and interconnect using ink-jet printing technology," *Journal of the Society for Information Display*, vol. 9, no. 1, pp. 9–13, 2001.

[27] H.-S. Koo, M. Chen, and P.-C. Pan, "Lcd-based color filter films fabricated by a pigment-based colorant photo resist inks and printing technology," *Thin solid films*, vol. 515, no. 3, pp. 896–901, 2006.

[28] J. Castrejón-Pita, G. Martin, S. Hoath, and I. Hutchings, "A simple large-scale droplet generator for studies of inkjet printing," *Review of Scientific Instruments*, vol. 79, no. 7, pp. 075 108–1;075 108–8, 2008.

[29] W. D. Wu, K. C. Patel, S. Rogers, and X. D. Chen, "Monodisperse droplet generators as potential atomizers for spray drying technology," *Drying Technology*, vol. 25, no. 12, pp. 1907–1916, 2007.

[30] A. A. Goghari and S. Chandra, "Producing droplets smaller than the nozzle diameter by using a pneumatic drop-on-demand droplet generator," *Experiments in Fluids*, vol. 44, no. 1, pp. 105–114, 2008.

[31] S. X. Cheng, T. Li, and S. Chandra, "Producing molten metal droplets with a pneumatic droplet-on-demand generator," *journal of materials processing technology*, vol. 159, no. 3, pp. 295–302, 2005.

[32] S. Chandra and R. Jivraj, "Apparatus and method for generating droplets," Sep. 10 2002, uS Patent 6,446,878.

[33] J. Luo, L.-h. Qi, J.-m. Zhou, X.-h. Hou, and H.-j. Li, "Modeling and characterization of metal droplets generation by using a pneumatic drop-on-demand generator," *Journal of Materials Processing Technology*, vol. 212, no. 3, pp. 718–726, 2012.

[34] J. F. Edd, M. Toner, D. DiCarlo, and D. Irimia, "Microfluidic droplet encapsulation," Jun. 30 2015, uS Patent 9,068,181.

[35] C. A. Stan, G. F. Schneider, S. S. Shevkoplyas, M. Hashimoto, M. Ibanescu, B. J. Wiley, and G. M. Whitesides, "A microfluidic apparatus for the study of ice nucleation in supercooled water drops," *Lab on a Chip*, vol. 9, no. 16, pp. 2293–2305, 2009.

[36] W. Engl, R. Backov, and P. Panizza, "Controlled production of emulsions and particles by milli-and microfluidic techniques," *Current Opinion in Colloid & Interface Science*, vol. 13, no. 4, pp. 206–216, 2008.

[37] J. Xu and D. Attinger, "Drop on demand in a microfluidic chip," *Journal of Micromechanics and Microengineering*, vol. 18, no. 6, pp. 065 020–065 030, 2008.

[38] S. Okushima, T. Nisisako, T. Torii, and T. Higuchi, "Controlled production of monodisperse double emulsions by two-step droplet breakup in microfluidic devices," *Langmuir*, vol. 20, no. 23, pp. 9905–9908, 2004.

[39] F. Sultan, N. Ashgriz, D. Guildenbecher, and P. Sojka, "Electrosprays," in *Handbook of Atomization and Sprays*. Springer, 2011, ch. 32, pp. 727–753.

[40] M. Cloupeau and B. Prunet-Foch, "Electrohydrodynamic spraying functioning modes: a critical review," *Journal of Aerosol Science*, vol. 25, no. 6, pp. 1021–1036, 1994.

[41] G. Zhang, L. Qian, J. Zhao, H. Zhou, and H. Lan, "High-resolution electric-field-driven jet 3d printing and applications," *3D Printing*, p. 23, 2018.

[42] J. Grace and J. Marijnissen, "A review of liquid atomization by electrical means," *Journal of aerosol science*, vol. 25, no. 6, pp. 1005–1019, 1994.

[43] D. Berlincourt, H. Jaffe, W. Merz, and R. Nitsche, "Piezoelectric effect in the ferroelectric range in sbsi," *Applied Physics Letters*, vol. 4, no. 3, pp. 61–63, 1964.

[44] R. F. Mould, "Pierre curie, 1859–1906," *Current oncology*, vol. 14, no. 2, pp. 74–82, 2007.

[45] W. P. Mason, "Piezoelectricity, its history and applications," *The journal of the Acoustical Society of America*, vol. 70, no. 6, pp. 1561–1566, 1981.

[46] K.-C. Fan, J.-Y. Chen, C.-H. Wang, and W.-C. Pan, "Development of a drop-on-demand droplet generator for one-drop-fill technology," *Sensors and Actuators A: Physical*, vol. 147, no. 2, pp. 649–655, 2008.

[47] D.-A. Wang and N.-Z. Liu, "A shear mode piezoelectric energy harvester based on a pressurized water flow," *Sensors and actuators A: Physical*, vol. 167, no. 2, pp. 449–458, 2011.

[48] W. D. Wu, S. X. Lin, and X. D. Chen, "Monodisperse droplet formation through a continuous jet break-up using glass nozzles operated with piezoelectric pulsation," *AIChE Journal*, vol. 57, no. 6, pp. 1386–1392, 2011.

[49] H.-B. Lin, J. Eversole, and A. Campillo, "Vibrating orifice droplet generator for precision optical studies," *Review of scientific instruments*, vol. 61, no. 3, pp. 1018–1023, 1990.

[50] G. Brenn, “Droplet stream generator,” in *Handbook of Atomization and Sprays*. Springer, 2011, pp. 603–624.

[51] A. V. Sergeyev and R. A. Shaw, “An inexpensive uniform-size aerosol generator,” *Measurement Science and Technology*, vol. 17, no. 10, pp. N41–N44, 2006.

[52] E. Li, Q. Xu, J. Sun, J. Fuh, Y. Wong, and S. T. Thoroddsen, “Design and fabrication of a pet/ptfe-based piezoelectric squeeze mode drop-on-demand inkjet printhead with interchangeable nozzle,” *Sensors and Actuators A: Physical*, vol. 163, no. 1, pp. 315–322, 2010.

[53] D. M. Harris, T. Liu, and J. W. Bush, “A low-cost, precise piezoelectric droplet-on-demand generator,” *Experiments in Fluids*, vol. 56, no. 4, p. 83, 2015.

[54] S. M. Inc. (2019, May) Steminc, steiner and martins inc. [Online]. Available: https://www.steminc.com/PZT/en/

[55] E. Optics. (2019, May) Edmund optics, worldwide. [Online]. Available: https://www.edmundoptics.eu/

Appendix A

.1 Data sheets of the used components

Table 1: Piezoelectric material properties.

”Electromechanical coupling coefficient”		
Kp	-	0.64
Kt	-	0.45
K31	-	0.37
Frequency constant		
Np	Hzm	2060
Nt	Hzm	2000
N31	Hzm	1500
Piezoelectric constant		
d33	$\times 10^{-}12$m/v	500
d31	$\times 10^{-}12$m/v	-210
g33	$\times 10^{-}3$Vm/N	24.2
g31	$\times 10^{-}3$Vm/N	-10.4
Elastic Constant		
Y33	$\times$1010N/m^2	5.4
Y11	$\times$1010N/m^2	7.4
Mechanical Quality Factor		
Qm	-	85
Dielectric Constant		
e^T33/e 0	@1 kHz	2100
Dissipation Factor		
tan δ	@1 kHz	2
Curie Temperature		
Tc	$^{\circ}$C	320
Density		
ρ	g/cm^3	7.8

Table 2: Specifications of the Power supply.

Output voltage	0 - 30 V DC
Output current	0 - 5 A
Output power	150 W
Residual ripple (U)	0,5 mV rms
Residual ripple (I)	3 mA rms
Operating voltage	115/230 V AC; 50/60 Hz
Dimension (WxHxD)	135 x 165 x 275 mm
Weight	5,5 kg
EAN-13	4250569401459

Table 3: Specifications of the LED ribbon.

Aperture angle	120º
Lifespan	30.000 H
Energetic class	A+
Certifications	CE & RoHS
Dimensions	18x5x5000 mm
IP Protection	IP67
Lighting source	SMD5050
Power	70 W
Power supply	12V DC